

# Ru-doped functional porous materials for electrocatalytic water splitting

Chongao Tian<sup>1</sup>, Rui Liu<sup>1</sup>, Yu Zhang<sup>2</sup>, Wenxiu Yang<sup>1</sup> (✉), and Bo Wang<sup>1</sup> (✉)

<sup>1</sup> Beijing Key Laboratory of Photoelectronic/Electrophotonic Conversion Materials, Advanced Technology Research Institute (Jinan), Advanced Research Institute of Multidisciplinary Science, School of Chemistry and Chemical Engineering, Beijing Institute of Technology, Beijing 100081, China

<sup>2</sup> Beijing Institute of Technology Library, Beijing Institute of Technology, Beijing 100081, China

© Tsinghua University Press 2023

Received: 21 June 2023 / Revised: 6 July 2023 / Accepted: 10 July 2023

## ABSTRACT

Electrolytic water splitting (EWS) is an attractive and promising technique for the production of hydrogen energy. Nevertheless, the sluggish kinetic rate of hydrogen/oxygen evolution reactions leads to a high overpotential and low energy efficiency. Up to date, Pt/Ir-based nanocatalysts have become the state-of-the-art EWS catalysts, but disadvantages such as high cost and low earth abundance greatly limit their applications in EWS devices. As an attractive candidate for the Pt/Ir catalysts, series of Ru-based nanomaterials have aroused much attention for their low price, Pt-like hydrogen bond strength, and high EWS activity. In particular, Ru-doped functional porous materials have been becoming one of the most representative EWS catalysts, which can not only achieve the dispersion and adjustment for active Ru sites, but also simultaneously solve the problems of mass transfer and catalytic conversion in EWS. In this review, the design and preparation strategies of Ru-doped functional porous materials toward EWS in recent years are summarized, including Ru-doped metal organic frameworks (MOFs), Ru-doped porous organic polymers (POPs), and their derivatives. Meanwhile, detailed structure–activity relationships induced by the tuned geometric/electronic structures of Ru-doped functional porous materials are further depicted in this review. Last but not least, the challenges and perspectives of Ru-doped functional porous materials catalysts are reasonably proposed to provide fresh ideas for the design of Ru-based EWS catalysts.

## KEYWORDS

Ru-based catalyst, functional porous materials, electrolytic water splitting, oxygen evolution reaction, hydrogen evolution reaction

## 1 Introduction

Hydrogen energy has been regarded as an attractive renewable energy due to its high gravimetric energy density (142 MJ·kg<sup>-1</sup>), zero-carbon-emissions, and wide-application [1]. Yet the current industrial hydrogen production technology is still dominated by foil-fuel-reforming process, which would release numerous CO<sub>2</sub> and decrease the purity of hydrogen [2]. As a clean and efficient hydrogen production technology, electrolytic water splitting (EWS) has been attracting much attention in recent years [3, 4]. Hydrogen evolution reaction (HER) and oxygen evolution reaction (OER) are the key cathode and anode steps for EWS, respectively. Nevertheless, the practical potential required in EWS is much higher than the theory value of 1.23 V, because of the existence of slow kinetics of HER and OER [5]. To date, Pt- and Ir/IrO<sub>2</sub>-based precious metal nanomaterials are excellent HER and OER electrocatalysts, respectively [6, 7]. However, their shortcomings such as high cost and low earth abundance greatly limit the development and large-scale applications of EWS devices. And the widely used commercial Pt/C also has the problems, such as high Pt loading and heterogeneous dispersion of Pt nanoparticles. Therefore, it is of great significance to explore low-price, efficient, and stable electrocatalysts to minimize the active

energy of HER/OER and ultimately prompt the efficiency of the EWS process.

As one of the Pt-group materials, Ru-based catalysts have become the alternative HER and OER catalysts for their high activity and Pt-like hydrogen bond strength [8, 9]. Meanwhile, the price of Ru is ~ 25 and ~ 7.5 times cheaper than those of Pt and Ir, respectively [10]. However, several issues still exist in Ru-based EWS electrocatalysts: (1) low Ru utilization efficiency; (2) insufficient stability due to the inevitable re-structure and dissociation of Ru; and (3) performance differences among Ru single atom, Ru clusters, and Ru nanoparticles supported catalysts [11–13]. Based on these issues, series of advanced strategies such as morphology/hierarchical pores/defect adjustment, surface/interface engineering, and electric structure regulation are accordingly proposed for Ru-based catalysts.

Supported Ru nanocatalysts are one of the most potential Ru-based catalysts for EWS. Remarkably, designing novel supports with excellent metal–support interaction (MSI) and preparing Ru single atom/clusters/nanoparticles anchored catalysts could rationally optimize the EWS performance to a big extent [14]. Generally, nanocarbon materials with high surface areas and abundant pores, such as graphene, fullerene, hollow mesoporous

Address correspondence to Wenxiu Yang, yangwx19@bit.edu.cn; Bo Wang, bowang@bit.edu.cn

carbon spheres, two-dimensional (2D) nanocarbon layer, and ordered macroporous carbon superstructure, are selected as supports to anchor Ru active sites by lattice-confinement, pore confinement, and coating confinement [15–23]. Thanks to the high surface area, abundant pores, and tuned MSI, these supported Ru nanocatalysts have achieved a comparable EWS performance to the Pt/Ir-based catalysts.

Functional porous materials such as microporous zeolites, metal organic frameworks (MOFs), and porous organic polymers (POPs) have attracted much attention in the area of catalysis, energy storage, and conversion thanks to their large specific surface area, controllable chemical composition, abundant active sites, and spatial confinement effects [24–29]. Especially in the EWS aspects, functional porous materials and their derivatives could be regarded as excellent supports to anchor the Ru species to optimize the MSI effect and enhance their EWS performance. For example, series of porous framework materials such as UiO-66-NH<sub>2</sub>, Ni-BDC, zeolitic imidazolate framework (ZIF)-67, and 2D-covalent organic frameworks (COFs) have been used for the design of Ru-doped functional porous materials. The advantages of these Ru-doped functional porous materials can be summarized as follows: (1) The MSI effect and stability of Ru-doped functional porous materials can be enhanced because of the confinement effect of functional porous materials for Ru species. (2) The utilization of Ru can be improved in Ru-doped functional porous materials, which can be attributed to the abundant Ru anchor sites provided by functional porous frameworks. (3) The highly versatile and well-defined porosity of functional porous materials is suited to electron transfer and mass transport of the Ru-doped functional porous materials. (4) The electronic configuration of Ru sites can be tuned in the Ru-doped functional porous materials system, ultimately optimizing the intrinsic catalytic activity of Ru. Among them, the similarities of these Ru-doped porous materials, such as the optimized mass transfer and enhanced metal utilization, can be ascribed to the well-defined porous structure and the uniformly dispersed Ru-based active sites simulated by the advantages of porous framework materials. And the differences of these Ru-doped porous materials in their electrocatalytic performance are attributed to the synergistic effect active Ru sites and porous framework materials.

To date, the reviews on Ru-based EWS catalysts mainly focused on metallic Ru-based nanomaterials or Ru single atom catalysts, and few reviews can give a comprehensive illustration of Ru-anchored functional porous frameworks EWS catalysts [30–34]. Therefore, it is essential to logically summarize the Ru-doped functional porous materials catalysts from preparation to geometric/electric structure adjustment, verifying the structure–activity relationships of these catalysts for EWS, so as to better reflect the similarity and difference of Ru-doped porous materials. In this review, the design and preparation of Ru-doped functional porous materials toward EWS in recent years are summarized, including Ru-doped MOFs, Ru-doped POPs, and their derivatives (Fig. 1). Meanwhile, the details about synthetic methods and structure–activity relationships are also depicted in this review. Last but not least, the challenges and perspectives of Ru-doped functional porous materials are reasonably proposed, aiming to provide fresh ideas for the design of Ru-based EWS catalysts.

## 2 Ru-doped MOFs and their derivatives

MOFs are a kind of functional porous crystalline materials assembled by metal ions/clusters and organic ligands through coordination bonds [35, 36]. Benefiting from their diversity of metals/ligands, large specific surface area, and adjustable porous

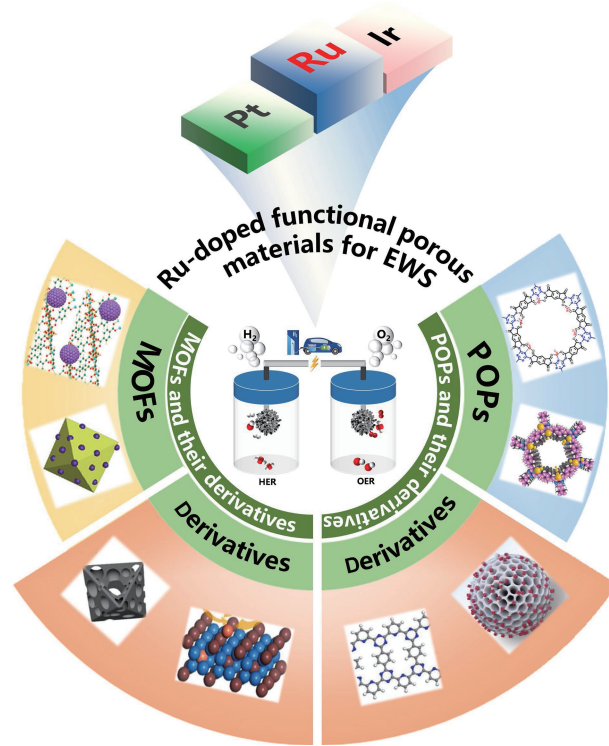


**Figure 1** Schematic illustration of the classification of Ru-doped functional porous materials for electrolytic water splitting.

structure, MOFs have been regarded as potential carrier or co-catalysts for the catalytic process [37]. In special, based on the requirement of EWS for active sites and mass/electron transfer channels, Ru-doped pristine MOFs have been gradually paid much attention in the past few years, where Ru single atoms, Ru nanoparticles, and Ru-based alloys can be successfully confined in MOFs by optimizing the synthetic methods. Meanwhile, series Ru-doped MOF derivatives including Ru-doped carbon composites and Ru-doped metal oxides/sulfides/phosphides have achieved excellent EWS performance, even at industrial current densities.

### 2.1 Ru-doped pristine MOFs electrocatalysts

With the uniformly dispersed metal sites, MOFs can be directly used as electrocatalyst in some electrocatalytic systems such as fuel cells, EWS, and CO<sub>2</sub> reduction reaction [46–48]. Meanwhile, the tuned ligand defects and porous structures of MOFs can also prompt the introduction of guest metal sites and further enhance their intrinsic activities. As for EWS, Ru-based species have been regarded as the potential active sites both in acidic and alkaline medium [49]. Therefore, it is of importance to explore efficient strategies to construct the Ru-doped pristine MOFs catalysts and analyze their structure–activity relationships, for example, Ru single atoms, Ru nanoparticles, and Ru-based alloys doped MOFs. By synergistic effect of MOFs and Ru, the EWS activity can be optimized in a big extent. Table 1 summarizes the related properties of Ru-doped pristine MOFs catalysts for electrocatalytic water splitting in recent years.

#### 2.1.1 Ru nanoparticles

Recently, series Ru nanoparticles supported catalysts have been designed for EWS benefitting from remarkable activity, which are usually composed of two crystal structures, either a hexagonal close packed (hcp) or an unusual face-centered cubic (fcc) structure [50–52]. The homogeneous dispersion of the Ru nanoparticles can result in wide exposure of the active sites, consequently improving electrocatalytic performance. However, bare Ru nanoparticles would gradually lose activity due to the

**Table 1** Electrocatalytic performance of Ru-doped pristine MOFs electrocatalysts

Materials	Electrolytes	HER $\eta$ (mV@mA·cm <sup>-2</sup> )	OER $\eta$ (mV@mA·cm <sup>-2</sup> )	Tafel slope (mV·dec <sup>-1</sup> )	Stability (mA·cm <sup>-2</sup> @h)	References
Ru@Ni-MOFs/NF	1 M KOH	25@–10	—	31	–10@80 h	[38]
Ru-NiFe-x/NF (1.6 at.% of Ru)	1 M KOH	90@–100	310@100	42.7 (HER) — (OER)	–50@20 h (HER) 100@24 h (OER)	[39]
Rh <sub>50</sub> Ru <sub>50</sub> @UiO-66-NH <sub>2</sub>	0.5 M H <sub>2</sub> SO <sub>4</sub>	177@–10	—	111.8	85%@20 h	[40]
	1 M PBS	77@–10	—	79	—	[40]
	1 M PBS	114@–10	—	93.4	72.3%@15 h	[40]
NiRu <sub>0.13</sub> -BDC/NF	1 M KOH	34@–10	—	32	–12@30 h	[41]
	1 M HCl	13@–10	—	—	—	[41]
NiRu <sub>0.08</sub> -MOF/NF	0.1 M KOH	—	187@10	40	40@300 h	[42]
NiRu-MOF/NF	1 M KOH	51@–10	—	90	–30@24 h	[43]
MIL-53(Ru-NiFe)@NF	1 M KOH	27@–10	210@50	49 (HER) 42 (OER)	–50@18 h (HER) 50@18 h (OER)	[44]
Ru-NiFe-MOF/NF	1 M KOH	—	205@10	50	10@100 h	[45]

corrosion in the catalytic process. In order to maintain high activity for a long time, carrier loading, surface encapsulation, and cage material encapsulation have been usually regarded as the reasonable methods [53]. In special, MOFs with abundant porous structure can effectively alleviate the loss of Ru nanoparticles, consequently enhancing the catalytic performance.

Li and co-workers fabricated Ru@Ni-MOFs/NF (NF = nickel foam) catalyst through solvothermal method (Fig. 2(a)), where NF not only acted as a conductive carrier, but also as reductant to convert Ru<sup>3+</sup> to metal Ru [38]. It can be seen that uniform dispersion of Ru nanoparticles (~ 4 nm) is in transmission electron microscopy (TEM) image (Fig. 2(b)). Furthermore, high-resolution TEM (HRTEM) image showed that the interplanar spacing was 0.23 nm, belonging to the (100) crystal facet of Ru (Fig. 2(c)). Significantly, an obvious interface structure with strong interaction could be noticed in Ru@Ni-MOFs/NF. As reported, this interface structure could electronically change the active sites to modify the bonding strength of the reaction intermediates, thereby improving the slow HER kinetics [54, 55]. The Ru–O bond was visible in X-ray photoelectron spectroscopy (XPS)

spectrum of Ru@Ni-MOFs/NF, indicating that Ru nanoparticles could be stably embedded in the framework by forming an interfacial bond between the edge of Ru nanoparticles and the carboxyl oxygen of Ni-MOFs, significantly enhancing the long-term stability of the catalyst. Moreover, the synergistic mechanism of HER on the as-prepared catalyst was concluded (Fig. 2(d)), which provided a new idea for the theoretical study of HER in alkaline media. Similarly, Wang and co-workers prepared a self-supported Ru-NiFe-x/NF electrode through spontaneous galvanic replacement reaction (GRR) (Fig. 2(e)) [39]. The whole process is a simple soaking without additional reducing agent at room temperature (RT), belonging to a thermodynamically promoted reaction. Benefiting from hierarchical flaky structure of NiFe-MOF raised catalytic efficacy of single active sites, Ru-NiFe/NF (1.6 at.% of Ru) exhibited outstanding HER/OER activity at high current density (Figs. 2(f) and 2(g)). In summary, the unique framework of MOFs can not only protect the loss of Ru nanoparticles, its intrinsic active sites are also beneficial to improve the electrocatalytic performance.

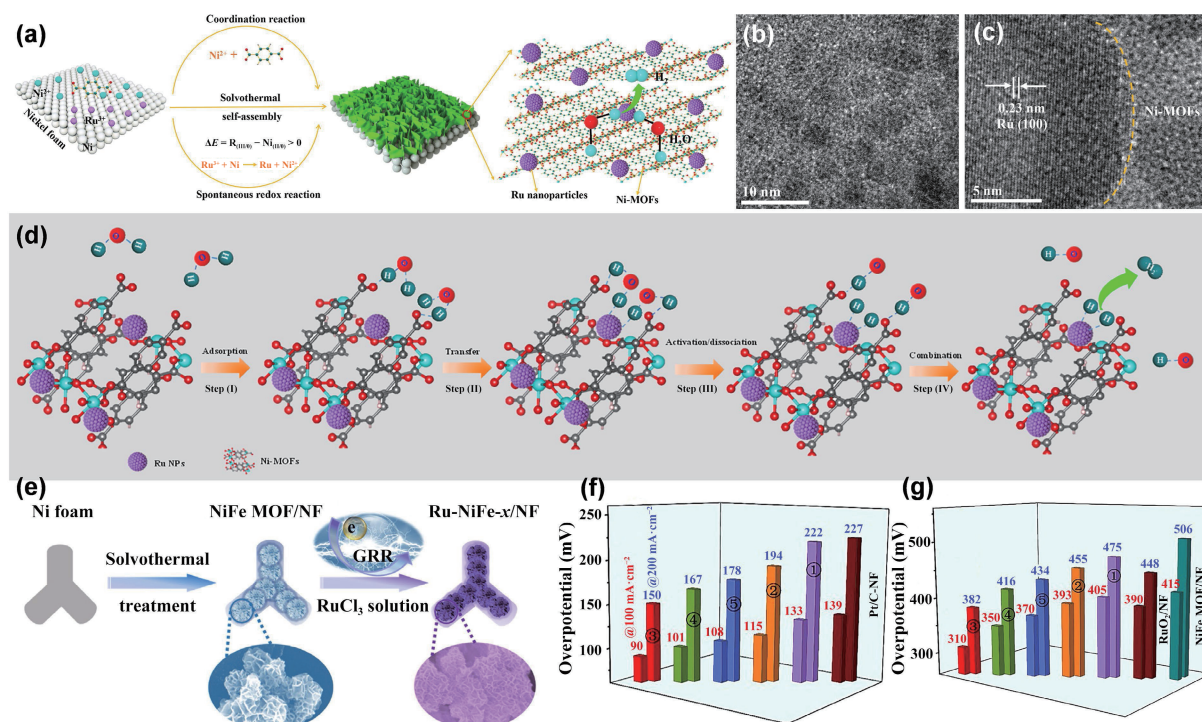


**Figure 2** (a) Synthetic process of Ru@Ni-MOFs/NF. (b) TEM image of Ru@Ni-MOFs/NF. (c) HRTEM image of Ru@Ni-MOFs/NF. (d) H<sub>2</sub>O synergistic dissociation mechanism on Ru@Ni-MOFs/NF toward HER. Reproduced with permission from Ref. [38], © Elsevier B.V. 2022. (e) Synthetic process of Ru-NiFe-x/NF. Overpotential of series of catalysts toward (f) HER and (g) OER. Reproduced with permission from Ref. [39], © Elsevier Inc. 2021.

### 2.1.2 Ru-based alloys

As is known, alloying hetero metal elements is an efficient method to regulate the surface/interface chemical properties of the host metal [56–59]. Based on this, the lattice parameters and charge dispersion can be efficiently optimized, which ultimately improve the electrocatalytic performance [60, 61]. As for Ru-precious metal alloys, Ru-Ir, Ru-Pt, and Ru-Pd alloys are firstly prepared as the EWS catalysts [62, 63]. Meanwhile, to further decrease the cost, series of Ru transition metals (Co, Ni, Fe, etc.)-based alloys have also been designed for EWS [64, 65]. Specially in the MOF supported Ru-based alloys catalysts, the adjustable pore structure of MOFs is favorable for the encapsulation of alloys, and metal nodes in MOFs can regulate the electronic environment of Ru active sites, resulting in the uniform dispersion of Ru-based alloys and enhanced EWS performance.

By picking Ru-Rh alloys as an instance, Ding and co-workers reported Rh-Ru alloyed nanoparticles embedded within the pores of UiO-66-NH<sub>2</sub> through *in situ* reduction toward HER in all pH values (Fig. 3(a)) [40]. In this report, the advantages of UiO-66-NH<sub>2</sub> are as follows: The larger pore diameter dispersion of UiO-66-NH<sub>2</sub> is suited to confine metal ions, and the amine groups on the organic linker can also coordinate with metal ions, which provides possibility for the successful anchoring of Ru-Rh alloys. TEM image showed that the spherical particles were homogeneously dispersed within the frameworks, suggesting that the alloy

nano-particles were successfully anchored in MOFs (Fig. 3(b)). Moreover, the *d*-spacing of 0.218 nm belonged to the crystal facet of RhRu (111) in HRTEM image, further verifying that Rh-Ru alloys were acquired (Fig. 3(c)). Remarkably, XPS spectra noticed that Rh 3d electrons had a lower binding energy in Rh<sub>50</sub>Ru<sub>50</sub>@UiO-66-NH<sub>2</sub> than in Rh<sub>100</sub>@UiO-66-NH<sub>2</sub>, while Ru 3p electrons had a slightly higher binding energy in Rh<sub>50</sub>Ru<sub>50</sub>@UiO-66-NH<sub>2</sub> than in Ru<sub>100</sub>@UiO-66-NH<sub>2</sub> (Figs. 3(d) and 3(e)). This phenomenon indicated that electron was transferred from Ru atom to Rh atom, which could potentially improve the electrocatalytic reaction kinetics and thus enhance the catalytic performance. Therefore, thanks to the synergetic effect of UiO-66-NH<sub>2</sub> supports, the optimization of electric structure of the resulting Rh<sub>50</sub>Ru<sub>50</sub>@UiO-66-NH<sub>2</sub> catalyst performed the best EWS activity at wide pH values compared to other contrast samples, which was prominently better than the commercial Ru/C.

### 2.1.3 Ru single atoms

With increasing attention given to single atom catalysts, isolated Ru single atoms dispersed on specific supports have been regarded as a new research frontier in EWS because of their maximum atomic utilization efficiency, higher mass activity, and unique quantum-size effect [66–69]. In special, Ru single atoms distributed on MOFs with high specific surface area have achieved outstanding EWS performance. Significantly, the strong

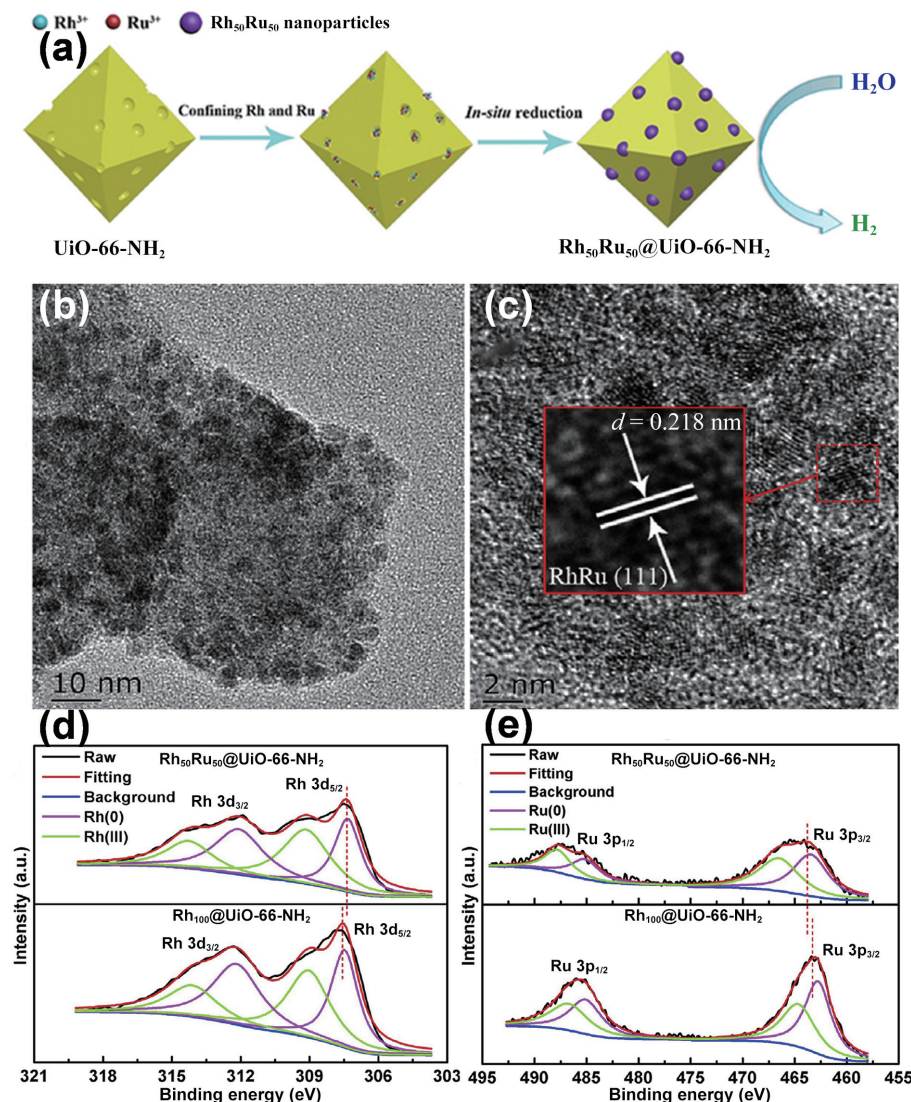


**Figure 3** (a) Synthetic process of Rh<sub>50</sub>Ru<sub>50</sub>@UiO-66-NH<sub>2</sub>, (b) TEM image and (c) HRTEM image of Rh<sub>50</sub>Ru<sub>50</sub>@UiO-66-NH<sub>2</sub>, (d) Rh 3d electrons and (e) Ru 3p electrons for Rh<sub>50</sub>Ru<sub>50</sub>@UiO-66-NH<sub>2</sub> and comparative samples. Reproduced with permission from Ref. [40], © Hydrogen Energy Publications LLC 2019.

interaction between Ru single atoms and MOFs can effectively modify the electronic structure of the active Ru catalytic sites and redistribute the local charge, which may regulate intermediate adsorption energy, contributing to the high EWS performance [43, 44].

Sun and co-workers designed an outstanding MOFs electrocatalyst ( $\text{NiRu}_{0.13}\text{-BDC}$ ) by introducing atomically dispersed Ru (Fig. 4(a)) [41]. Notably,  $\text{NiRu}_{0.13}\text{-BDC/NF}$  performed outstanding HER activity at all pH values, particularly in 1 M phosphate buffered saline (PBS) solution, with a low overpotential of 36 mV at 10 mA·cm<sup>-2</sup>, comparable to the commercial Pt/C. Moreover, compared with Ru foil and  $\text{RuO}_2$ , there are no evident characteristic peaks belonging to the Ru–Ru metal bond in the extended X-ray absorption fine structure (EXAFS) spectrum of  $\text{NiRu}_{0.13}\text{-BDC/NF}$ , indicating that Ru single atoms are successfully dispersed in Ni-BDC (Fig. 4(b)). In addition, density functional theory (DFT) calculations were performed to explore the effect of Ru single atoms on HER performance. Briefly, Ru in  $\text{NiRu}_{0.13}\text{-BDC}$  showed the lowest adsorption energy of  $\text{H}_2\text{O}$  ( $\Delta G_{\text{H}_2\text{O}^*}$ ), suggesting the strongest water absorption, which facilitates the next generation of adsorbed H atoms [70]. Moreover, the  $\Delta G_{\text{H}^*}$  of Ni was closer to 0, indicating that the adsorption of H was moderate, beneficial to H desorption and  $\text{H}_2$  release. Hence, the single atom Ru plays an important role in regulating metal centers of MOFs, contributing to water adsorption and  $\text{H}_2$  release, and thereby improving HER performance. Similar to Sun's method, Li and co-workers prepared  $\text{NiRu}_x\text{-MOF/NF}$  loaded with atomically dispersed Ru on Ni foam through hydrothermal method and ions substitution reaction (Fig. 4(c)), with an overpotential of 187 mV at 10 mA·cm<sup>-2</sup> and a Tafel slope of 40 mV·dec<sup>-1</sup> [42].  $\text{NiRu}_{0.08}\text{-MOF}$  only showed one primary peak in EXAFS spectrum, which could be attributed to Ru–O, verifying that Ru presented a single atom state in MOFs (Fig. 4(d)). The OER performance of the catalyst was explored by DFT calculations, and the  $\text{NiRu}_{0.08}\text{-MOF}$  catalyst could perform lower intermediate adsorption energy than pristine Ni-MOF in the OER process. In addition,  $\text{NiRu}_{0.08}\text{-MOF}$  had a higher density of states near the Fermi level, indicating improved conductivity of  $\text{NiRu}_{0.08}\text{-MOF}$ , beneficial to electrocatalytic properties.

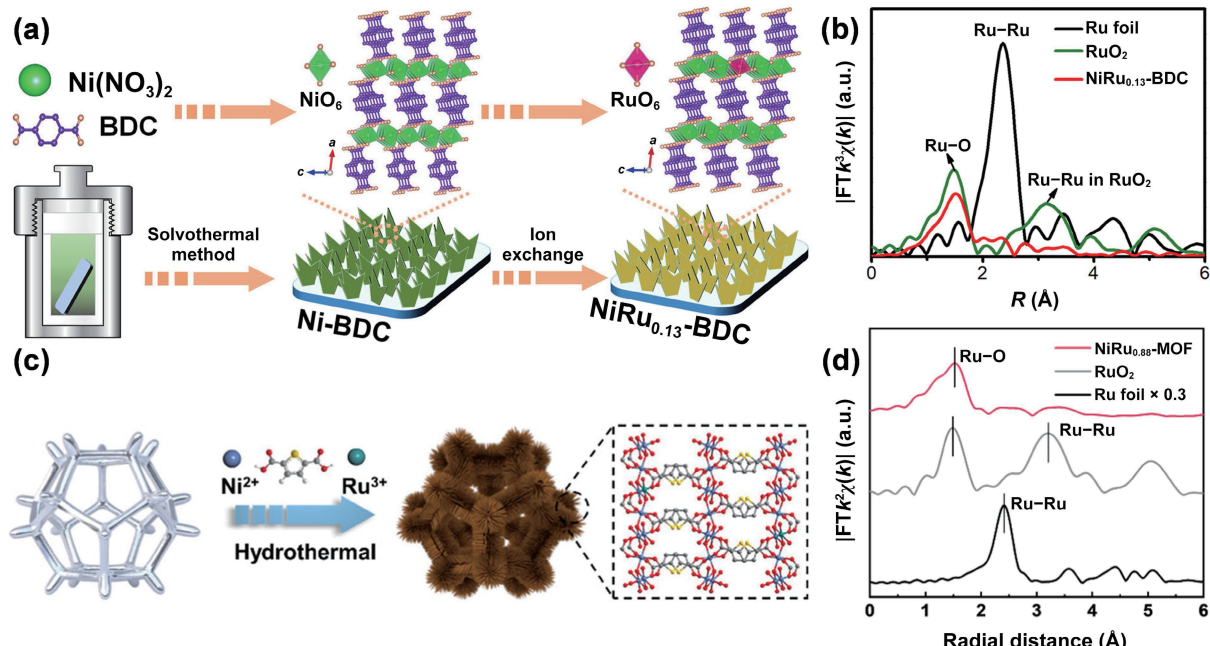


**Figure 4** (a) Synthesis of  $\text{NiRu}_{0.13}\text{-BDC/NF}$ . (b) Fourier transformed EXAFS spectra of  $\text{NiRu}_{0.13}\text{-BDC}$ . Reproduced with permission from Ref. [41], © Sun, Y. M. et al. 2021. (c) Synthesis of  $\text{NiRu}_{0.08}\text{-MOF/NF}$ . (d) Fourier transformed Ru K-edge EXAFS spectra of  $\text{NiRu}_{0.08}\text{-MOF}$ . Reproduced with permission from Ref. [42], © Li, Y. W. et al. 2022.

## 2.2 Ru-doped MOF derivatives electrocatalysts

In addition to the direct utilization of pristine MOFs as EWS electrocatalysts, MOF derivatives have been extensively reported as outstanding catalysts toward EWS benefitting from high electrical conductivity, great chemical stability, and extraordinary activity. Considering that synergistic effect of Ru and MOF derivatives can enhance EWS performance, Ru-doped MOF derivatives have been regarded as an effective strategy to prepare the EWS catalysts, such as Ru-doped MOF-derived carbon-based materials and MOF-derived metal oxides/sulfides/phosphides. Detailed synthetic methods and structure–activity relationships are shown as follows.

### 2.2.1 MOF-derived carbon-based materials

In 2008, MOFs were firstly reported as precursors for the synthesis of porous carbon. Since then, pyrolysis of MOFs has been recognized as an effective method to acquire carbon-based materials with various morphologies and compositions [90]. During the pyrolysis process, the organic ligands are converted into highly conductive porous carbon skeletons, meanwhile, the metal nodes transform into metal nanoparticles, metal compound nanoparticles, or single atoms that are uniformly dispersed within the carbon frameworks. In addition to the pristine metal nodes of MOFs, different metal sites can also be introduced in the pristine MOFs based on the need of electrochemical reactions. As is known, Ru metal are seen as active sites for HER and OER. Series of Ru doped MOFs precursors can be pre-designed for the preparation of MOF-derived Ru-C hybrids, which have been extensively applied in the aspect of EWS. For the application in OER/HER electrocatalysts, MOF-derived Ru-C hybrids are featured with the following advantages: (1) The carbon framework exhibits a large specific surface area, excellent electron/mass transfer, and good conductivity, which is beneficial to the uniform distribution of Ru active sites. (2) The incorporation of heteroatoms (e.g., N and Cl) in ligands of MOFs facilitates doping of carbon materials. Meanwhile, Ru is coupled with the metal center of MOFs to improve the electronic environment of the metal atoms, optimize the adsorption free energy, and enhance the catalytic performance. (3) The morphology and porosity of carbon support could be adjusted by exploring the post-treatment



清华大学出版社



Springer | www.editorialmanager.com/nare/default.asp

methods for MOFs. Herein, a summary of the performance of MOF-derived carbon-based materials toward EWS is shown in Table 2.

**Ru nanoparticles.** Generally speaking, metal nodes of MOFs are mostly transformed into metal nanoparticles that are uniformly dispersed within the carbon frameworks during the pyrolysis. For example, Qiu's group obtained ultrafine Ru nanoparticles supported on hierarchical porous carbon (Ru-HPC) by pyrolysis and etching using bimetallic MOFs as a template (Fig. 5(a)) [71]. As shown in Fig. 5(b), scanning electron microscopy (SEM) images showed that there were a large amount of macropores and mesopores derived from the inherent porosity of MOFs and the removal of Cu. And ultrafine Ru nanoparticles (~ 2.87 nm) were highly exposed within carbon substrates (Fig. 5(c)). Notably, Ru-HPC performed efficient HER activity in alkaline solution, with an overpotential of 22.7 mV at 25 mA·cm<sup>-2</sup> and a Tafel slope of 33.9 mV·dec<sup>-1</sup> (Fig. 5(d)). In view of the excellent HER performance of Ru-HPC, it was annealed in air and P-RuO<sub>2</sub> with better performance than commercial RuO<sub>2</sub> was obtained (Fig. 5(e)). To summarize, the removal of Cu particles produces plentiful meso/macropores, resulting in a mass of exposed Ru active sites in catalytic process.

Similarly, Hong and co-workers fabricated Ru-based hierarchical porous carbon for overall water splitting (Fig. 6(a)) [72]. The prepared HP-Ru/C had a unique hierarchical pore network, including abundant micro/meso/macropores, which significantly promoted the exposure of active sites and transfer of charge/mass. In addition, Yang's group provided different routes to prepare Ru/RuO<sub>2</sub> nanoparticles supported hierarchical porous

carbon materials (Ru/RuO<sub>2</sub>/HPC), where HCl and FeCl<sub>3</sub> were regarded as the etching agents to remove the CuO or Cu nanoparticles (Figs. 6(b) and 6(c)) [73]. As a result, the high electrocatalytic OER activity could be achieved in obtained Ru/Cu-doped RuO<sub>2</sub>@HPC structure with an overpotential of 204 mV at 10 mA·cm<sup>-2</sup>. Through the analysis of the structural, compositional, and electrochemical results, the enhanced EWS property of catalyst can be ascribed to the high exposure of the ultrafine Ru/RuO<sub>2</sub> active sites and electronic modulation of Cu dopants.

**Ru-based alloys.** During the carbonization process, Ru and the metal nodes of MOFs can generate carbon-supported Ru-metal alloys through an ions substitution reaction, which exhibit significant electrocatalytic properties due to the electronic coupling of different metals and conductive carrier [78]. By picking Ru-Co alloys as instance, RuO<sub>2</sub>/Co<sub>3</sub>O<sub>4</sub>-RuCo@NC composites were obtained through the pyrolysis of ZIF-67 and followed by introducing Ru via GRR (Fig. 7(a)) [74]. The lattice distances enlarged HRTEM images and corresponding fast Fourier transformation (FFT) patterns suggested that Ru-Co alloy exhibited synergistic interfaces with Co<sub>3</sub>O<sub>4</sub> and RuO<sub>2</sub>, respectively (Figs. 7(b)–7(e)). It was the introduction of the metal–oxide interface that produced the Mott–Schottky effect and hence promoted the charge transfer in the electrocatalytic reaction. Benefiting from the protection of the carbon framework, the composites perform the remarkable performance in acidic solution with an overpotential of 247 mV at 10 mA·cm<sup>-2</sup>. And it was more stable than commercial RuO<sub>2</sub> and had outstanding charge transfer ability and fast OER kinetics. In summary, the retained carbon framework as a protective skeleton can not only

**Table 2** Electrocatalytic performance of MOF-derived carbon-based materials

Materials	Electrolytes	HER $\eta$ (mV@mA·cm <sup>-2</sup> )	OER $\eta$ (mV@mA·cm <sup>-2</sup> )	Tafel slope (mV·dec <sup>-1</sup> )	Stability (mA·cm <sup>-2</sup> @h)	References
Ru-HPC	1 M KOH	22.7@–25	—	33.9	–5@10 h	[71]
	1 M KOH	25@–10	—	29	–10@8 h	
HP-Ru/C	0.5 M H <sub>2</sub> SO <sub>4</sub>	38@–10	—	39	–10@–12 h	[72]
	1 M PBS	52@–10	—	52	–10@11 h	
Ru/Cu-doped RuO <sub>2</sub>	1 M KOH	28@–10	204@10	35 (HER) 56 (OER) 63 (HER) 89 (OER) 106 (HER)	36 mV@11h 226 mV@5 h –10@14 h (HER) 10@8 h (OER)	[73]
RuO <sub>2</sub> /Co <sub>3</sub> O <sub>4</sub> -RuCo@NC	0.5 M H <sub>2</sub> SO <sub>4</sub>	141@–10	247@10	—	—	[74]
RuCo@C-350	1 M KOH	91@–19	230@10	110 (OER)	—	[75]
RuCo@NC	1 M KOH	28@–10	—	31	—	[76]
Ru-Co@C	1 M KOH	—	330@10	60.4	500 mV@10 h	[77]
RuCo@NC	1 M KOH	40@–10	280@10	54 (HER) 91 (OER)	330 mV@20 h (OER)	[78]
CoRu-O/A@HNC	1 M KOH	85@–10	234@10	72.5 (HER) 63.8 (OER)	–50@48 h (HER) 10@8 h (OER)	[79]
NiRu@N-C	1 M KOH	32@–10	—	64	–10@10 h	[80]
	0.5 M H <sub>2</sub> SO <sub>4</sub>	50@–10	—	36	10@10 h	
Ni@Ru/CNS-10%	1 M KOH	20.1@–10	—	—	—	[81]
	0.5 M H <sub>2</sub> SO <sub>4</sub>	65.6@–10	356@10	56.9 (HER) 81.9 (OER)	77 mV@15 h (HER) 10@20 h (OER)	
Mo@Ru-3	0.1 M PBS	330.3@–10	—	—	—	
Ru-Cu@C-2	0.5 M H <sub>2</sub> SO <sub>4</sub>	30.5@–10	—	36.4	–20@10 h	[82]
Ru-Cu@C-2	1 M KOH	20@–10	—	37	—	[83]
Ru-Cl-N SAC	1 M KOH	12@–10	233@10	23.9 (HER) 196 (OER)	–20@120 h (HER) 10@120 h (OER)	[84]
Ru-NPs/SAs@N-TC	1 M KOH	97@–10	—	58	–1.0@14 h	[85]
Ru/3DMNC	1 M KOH	51@–10	—	60.1	–10@80 h	[86]
RuO <sub>2</sub> /3DMNC	1 M KOH	—	216.7@10	63.5	20@80 h	[86]
Sn <sub>0.1</sub> -RuO <sub>2</sub> @NCP	0.5 M H <sub>2</sub> SO <sub>4</sub>	—	178@10	60.6	10@150 h	[87]
Ru-MoO <sub>2</sub>	1 M KOH	29@–10	—	31	–10@2 h	[88]
	0.5 M H <sub>2</sub> SO <sub>4</sub>	59@–10	—	44	–20@20 h	
Ru/RuO <sub>2</sub> /CuCoN@NC-HS	1 M KOH	41@–10	231@10	45 (HER) 81 (OER)	140 mV@16 h (HER) 50@18 h (OER)	[89]

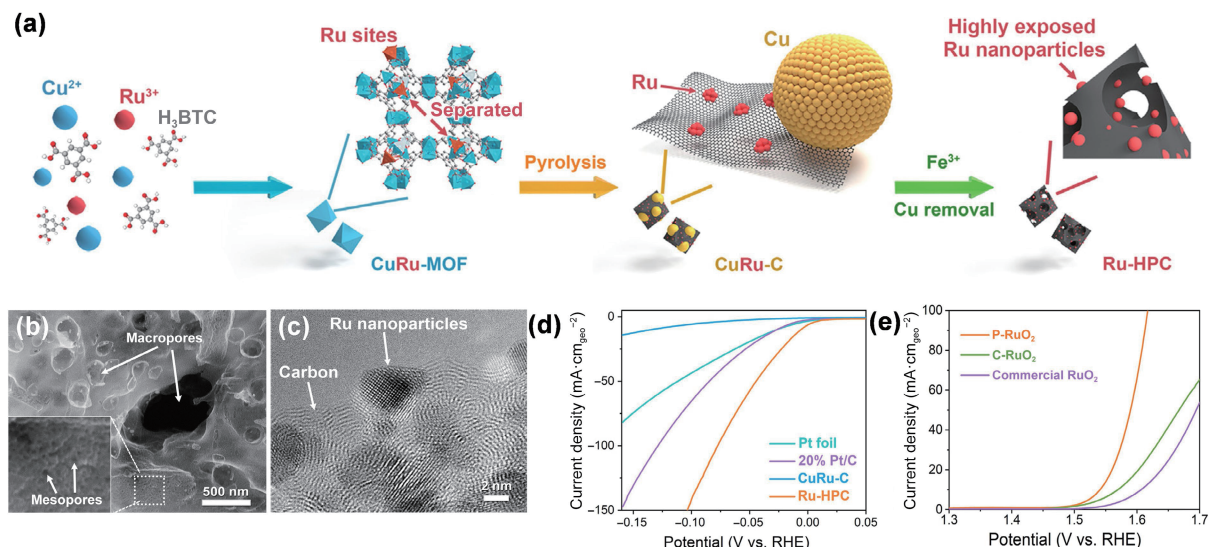


**Figure 5** (a) Synthesis of Ru-HPC. (b) SEM images of Ru-HPC. (c) HRTEM image of Ru-HPC. (d) Polarization curves of Ru-HPC in 1 M KOH solution. (e) Polarization curves of P-RuO<sub>2</sub> in 1 M KOH solution. Reproduced with permission from Ref. [71], © Elsevier Ltd. 2019.

prevent the aggregation and corrosion of metal components but also serve as an active site regulator to promote the adsorption of intermediates by redistributing charge and spin density. Moreover, Xu and co-workers prepared ultrafine RuCo nanoparticles confined within three-dimensional nitrogen-doped porous carbon from ZIF-67 and Ru species (Fig. 7(f)) [75]. The unique nanocage structure can provide more sites for the intermediate. And the doping of Ru could vastly induce the formation of heterostructures and the modulation of electronic structure, consequently promoting the active sites and intermediate binding energy of the catalyst. Besides, Su's group prepared a highly efficient and stable electrocatalyst composed of Ru and Co bimetallic nanoalloys encapsulated in nitrogen-doped graphene layers (Figs. 7(g) and 7(h)) [76]. In this system, the RuCo nanoalloys can be rapidly covered by graphene layers, effectively avoiding the agglomeration of alloy particles, and enhancing the catalytic activity and durability for HER.

Additionally, other Ru-transition metals alloys (such as Ru-Ni, Ru-Mo, and Ru-Cu) have also achieved remarkable EWS performance. Xu and co-workers prepared NiRu alloys nanoparticles encapsulated in nitrogen-doped carbon with low Ru contents (Fig. 8(a)) [80]. Benefiting from structural advantages and component synergy, the NiRu@N-C catalyst performed extraordinary HER activity in both acidic and alkaline solutions, almost equivalent to the commercial Pt/C (Figs. 8(b) and 8(c)). Moreover, Zhang's group reported the Mo@Ru electrocatalyst and investigated Mo modulation effect on Ru sites for the HER (Fig. 8(d)) [82]. The effect of Mo doping on the hydrogen binding energy and HER activity of catalyst was evaluated by DFT calculations. The Ru sites in MoRu<sub>3</sub> (Fig. 8(e)) performed a satisfactory  $\Delta G_{\text{H}^+}$ . Meanwhile, Mo sites in MoRu<sub>3</sub> exhibited a lower  $\Delta G_{\text{H}^+}$ , which was very close to that of Pt, indicating that the adsorption of H was moderate, beneficial to gas transfer and consequently enhancing EWS performance. In view of relatively great activity and stability, membrane electrode assembly (MEA) was prepared with Mo@Ru-3 catalyst as cathode and IrO<sub>2</sub> as anode, and tested in a single cell of PEM electrolyzer (Fig. 8(f)). As a result, at 80 °C, a current density of 1.0 A·cm<sup>-2</sup> was achieved at 1.95 V (Fig. 8(g)), superior to that of the electrolyzers in previous researches.

**Atomical Ru.** The atomic distribution of metal catalysts on the substrates could improve the utilization efficiency of active sites to a big extent [91–93]. To further expose Ru active sites, atomical Ru-doped MOF-derived carbon materials have been accordingly

prepared and performed extraordinary EWS activity. Considering that nitrogen atoms can anchor metal ions in carbon materials to form metal-N<sub>x</sub>C coordination structure, precursors of MOFs with nitrogen-containing organic connectors are preferred to efficiently convert metal nodes into atomically dispersed sites on carbon substrate [94, 95]. For instance, Chen and co-workers prepared RuCo-ZIF-67 and followed by pyrolysis, subsequently etched cobalt nanoparticles and unstable Ru species, finally Ru coordinated with Cl and N single atom catalyst (Ru-Cl-N SAC) was obtained (Fig. 9(a)) [84]. The image of aberration-corrected the high-angle annular dark-field scanning TEM (HAADF-STEM) indicated that Ru might appear mostly in the state of single atom. The single atomic Ru was marked by yellow arrows and Ru nanoparticles by yellow circles (Fig. 9(b)). Moreover, as depicted in Fig. 9(c), the peak located at 1.97 Å belonged to Ru-Cl bond and the peak located at 1.5 Å could be assigned to Ru-N bond, suggesting that Ru was successfully coordinated with Cl and N atoms. Benefiting from atomic active sites on the porous carbon substrate, the catalyst performed remarkable activity and stability toward HER/OER (Figs. 9(d) and 9(e)). In brief, Ru active species can be uniformly dispersed by the carbon framework, consequently improving the utilization of Ru. Meanwhile, the doping of heteroatoms improves the coordination environment of Ru atoms and optimizes the adsorption energy, beneficial to enhance electrocatalytic performance. Moreover, Yan's group prepared Ru-NPs/SAs@N-TC and Ru-SAs@N-TC catalysts utilizing NH<sub>2</sub>-MIL-125(Ti) derived N-doped TiO<sub>2</sub>/C as carrier (Fig. 9(f)) [85]. Ru species can be firmly supported with the help of the stabilization effects of uncoordinated groups and inherent pore-confinement of MOFs. Moreover, it was found that the doping amount of Ru<sup>3+</sup> ions not only affected the dispersed state of Ru species, but also determined the morphology and defect structure of N-TC carrier.

## 2.2.2 MOF-derived metal oxides/sulfides/phosphides

As is known, RuO<sub>2</sub> is the common material for OER in acidic solution due to the great activity and corrosion resistance. However, the reported OER performance of RuO<sub>2</sub>-based electrocatalysts in acidic solutions is still much lower than those in alkaline solutions. Benefiting from the protection of unique pores and the electronic regulation of metal nodes of MOFs, MOF-derived RuO<sub>2</sub> exhibits higher activity and durability than pure RuO<sub>2</sub>. Meanwhile, MOF-derived metal sulfides/phosphides also perform excellent EWS performance, which might be attributed to

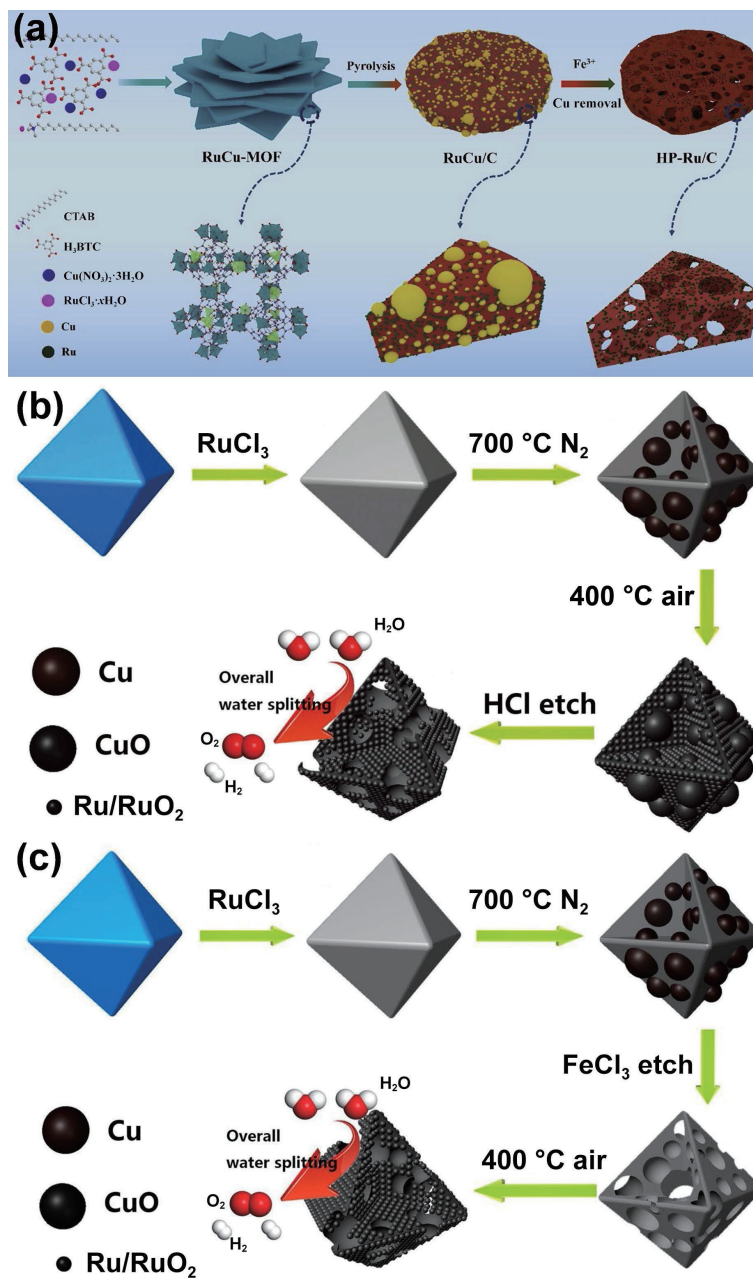


**Figure 6** (a) Synthetic process of HP-Ru/C. Reproduced with permission from Ref. [72], © Elsevier B.V. 2021. (b) Fabrication of Ru/Cu-doped RuO<sub>2</sub> supported hierarchical porous carbon. (c) Fabrication of Ru doped RuO<sub>2</sub> supported hierarchical porous carbon. Reproduced with permission from Ref. [73], © WILEY-VCH Verlag GmbH & Co. KGaA, Weinheim 2018.

the following factors: As for HER, heteroatoms (e.g., P and S) take electrons from the metal nodes of MOFs, resulting in the formation of negatively charged heteroatoms. These heteroatoms can be regarded as active sites for attachment and detachment of H atoms. As for OER, the delocalization of electrons between adsorbed oxygen, metal centers, and electronegative heteroatoms can promote the generation of OOH\* from OH\* [24]. A summary of the performance of MOF-derived metal oxides/sulfides/phosphides toward EWS is shown in Table 3.

Su and co-workers reported Cu-doped RuO<sub>2</sub> hollow porous polyhedra composed of ultrasmall nanocrystals by annealing of the Ru-doped Cu-BTC derivative (Fig. 10(a)) [96]. Based on thermogravimetry/differential thermal analysis (TG/DTA) and X-ray diffraction (XRD), the author inferred chemical phase transformation of annealed products. During the annealing process, the breakdown and oxidation of precursors will generate RuO<sub>2</sub> (Fig. 10(b)). Meanwhile, the reduction of parts of RuO<sub>2</sub> by the remnant organics could produce some metallic Ru species. In

brief, copper doping could adjust the electronic structure to improve activity and induce the production of unsaturated Ru sites, significantly improving the performance of RuO<sub>2</sub> (Fig. 10(c)). Similarly, Zhang's group prepared Zn-doped RuO<sub>2</sub> hollow nanorods by the same method (Figs. 10(d) and 10(e)) [97]. It was found that OER performance of RuO<sub>2</sub> can be effectively regulated by changing the amount of Zn species. The as-prepared RuO<sub>2</sub> catalyst with the 6.4 at.% Zn dopants (#2.5-S300) exhibited better electrocatalytic performance toward OER than commercial RuO<sub>2</sub> in acidic solution, with an overpotential of 206 mV at 10 mA·cm<sup>-2</sup> (Fig. 10(f)). And after 30 h chronopotentiometry test, the catalyst still maintained relatively high activity, better than the commercial RuO<sub>2</sub>. In addition, a low Ru contents oxide material (Cr<sub>0.6</sub>Ru<sub>0.4</sub>O<sub>2</sub>) derived from MOFs with outstanding OER performance was fabricated, which showed a low overpotential of 178 mV at 10 mA·cm<sup>-2</sup> and a long-term chronopotentiometry test at 10 mA·cm<sup>-2</sup> for 10 h in acidic solution [98]. It is worth noting that the direct annealing of MIL-101 (Cr) precursor only resulted in

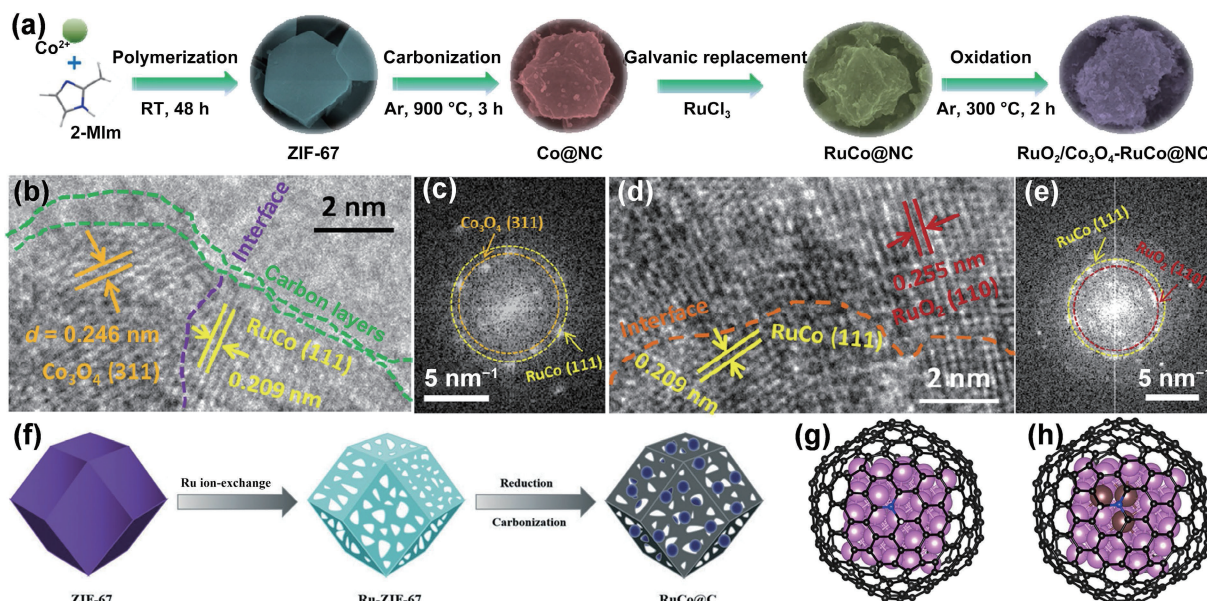


**Figure 7** (a) Synthetic process of RuO<sub>2</sub>/Co<sub>3</sub>O<sub>4</sub>-RuCo@NC. Enlarged HRTEM images and FFT patterns in ((b) and (c)) section I and ((d) and (e)) section II. Reproduced with permission from Ref. [74], © American Chemical Society 2019. (f) Synthetic process of RuCo@C. Reproduced with permission from Ref. [75], © The Royal Society of Chemistry 2022. (g) Pure Co model. (h) Ru<sub>3</sub>Co alloy model. The black, blue, pink, brown, and white balls refer to C, N, Co, Ru, and H atoms, respectively. Reproduced with permission from Ref. [76], © Su, J. W. et al. 2017.

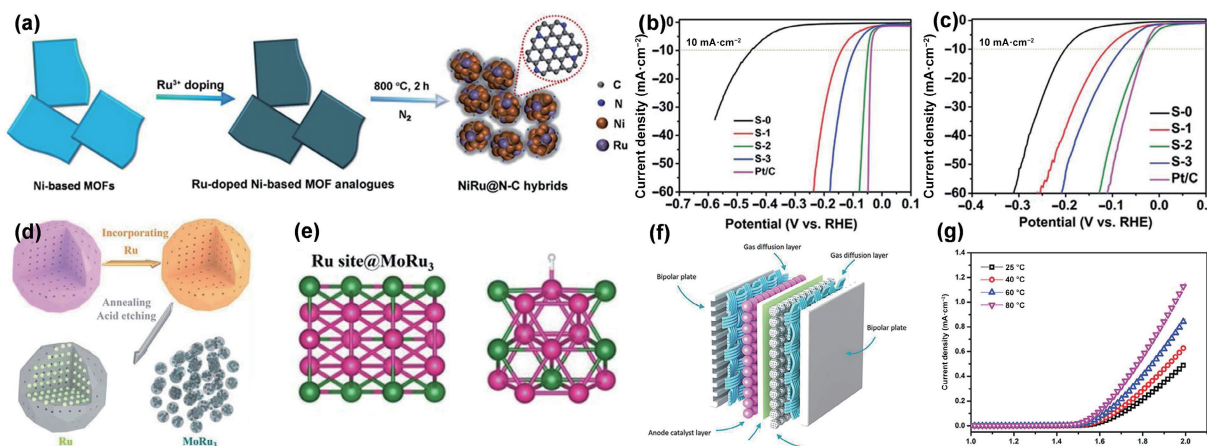


**Figure 8** (a) Synthesis of NiRu@N-C nanohybrids. Polarization curves of various NiRu@N-C in (b) acidic solution and (c) alkaline solution. Reproduced with permission from Ref. [80], © The Royal Society of Chemistry 2018. (d) Synthetic process of Mo@Ru catalyst. (e) The optimized adsorption structures of H\* on Mo site for MoRu<sub>3</sub>. (f) Scheme of PEM electrolyzer device. (g) Polarization curves for the PEM electrolyzer at different temperature. Reproduced with permission from Ref. [82], © The Royal Society of Chemistry 2019.

inactive Cr<sub>2</sub>O<sub>3</sub> product not active CrO<sub>2</sub>, suggesting that Ru took a crucial role in the formation of rutile-structured CrO<sub>2</sub> and CrO<sub>2</sub>-RuO<sub>2</sub> solid solutions.

As for MOF-derived metal sulfides/phosphides, it was found that a great deal of transition metal sulfides/phosphides had been reported as fascinating overall water splitting catalysts thanks to their hydrogenase-like catalytic mechanisms [104–106]. For instance, Lin and co-workers reported a ultra-low Ru (0.6 wt.%) doped bimetallic phosphide/NF hybrids (Ru-NiFeP/NF) from MIL-53(NiFe)MOF nanosheets through hydrothermal and phosphorization process (Fig. 11(a)) [101]. The Ru doping and phosphorization process can optimize the electronic structure, enhance the conductivity, and provide more catalytic active sites for HER and OER. As a result, the Ru-NiFeP/NF electrode only needed 1.47 V to produce 10 mA·cm<sup>-2</sup> in the assembled two-electrode alkaline electrolytic cell. Shen's group prepared Cu-doped RuS<sub>2</sub>/Ru heterostructure via sulphidation of RuCu-BTC followed by annealing process [102]. The simulation results of the theoretical model confirmed that H<sub>2</sub>O were more inclined to adsorb on the Cu sites in Cu-doped RuS<sub>2</sub>. And the thermodynamically stable adsorption sites of the H<sub>ads</sub> were on the

Ru atom (Figs. 11(b) and 11(c)). Furthermore, Cu-doped RuS<sub>2</sub> exhibited stronger water molecule binding ability than pure RuS<sub>2</sub>, which can effectively promote the water dissociation (Fig. 11(d)). And the  $\Delta G_{H^*}$  of Cu-doped RuS<sub>2</sub> was closer to 0 eV, which was helpful for H desorption and H<sub>2</sub> release (Fig. 11(e)). In brief, the Cu-doped RuS<sub>2</sub>/Ru catalyst performs better electrocatalytic activity, higher current density, and better stability, compared to the pristine RuS<sub>2</sub>. This is attributed to the synergistic effect of three-dimensional hollow structure, heterogeneous interface, and modulated electronic structure of Ru/Cu species.

### 2.2.3 Ru-doped other MOF derivatives

Generally, to solve the stability and conductivity issues of the Ru-doped pristine MOFs, pyrolysis under different gases (air, N<sub>2</sub>, NH<sub>3</sub>, etc.) is accordingly designed. However, the pyrolysis strategy always needs large energy consumption, and sometimes leads to damage the composition and structure of the pristine MOFs. Hence, it is important to explore novel non-pyrolysis procedures, such as defect engineering [113, 114], partially etching of MOFs [107], introducing active carriers, and microwave [115]. These synthetic methods are mild, easy to operate, and environmentally

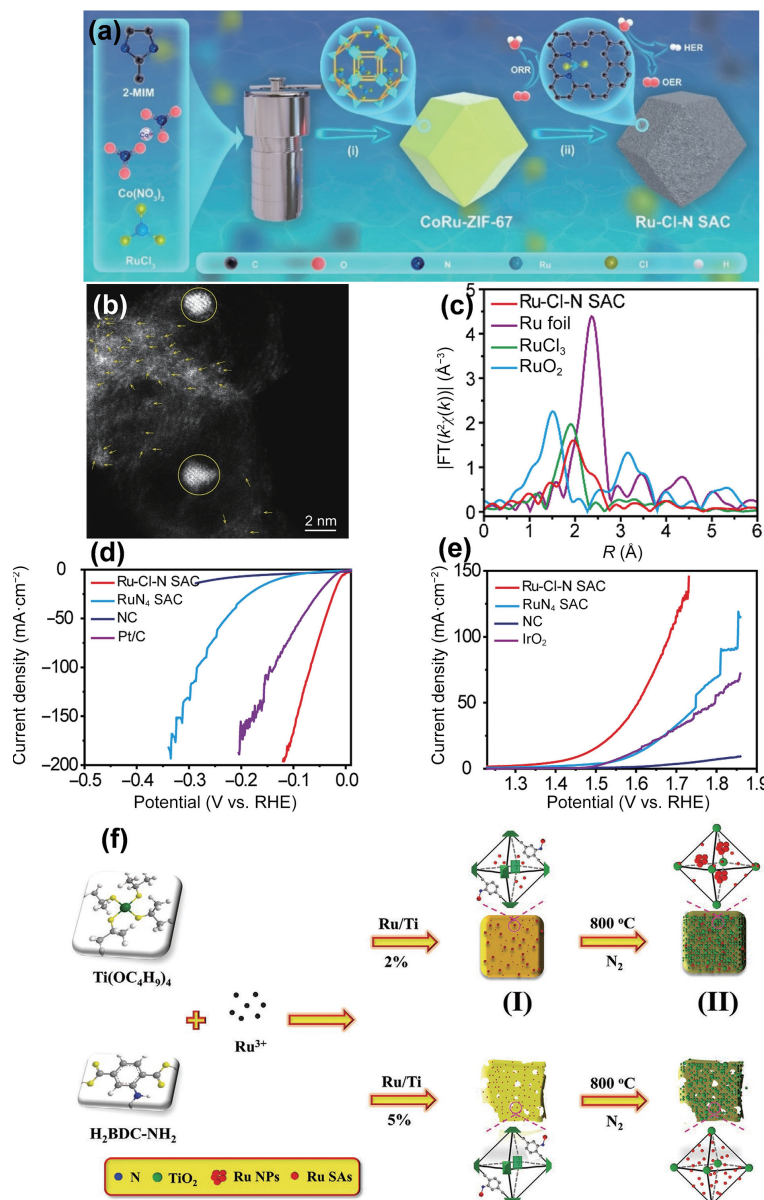


**Figure 9** (a) Fabrication of Ru-Cl-N SAC. (b) HAADF-STEM image of Ru-Cl-N SAC. (c) Ru K-edge EXAFS of Ru-Cl-N SAC. (d) Polarization curves of HER and (e) OER in 1 M KOH solution. Reproduced with permission from Ref. [84], © Elsevier B.V. 2022. (f) Synthesis of Ru-NPs/SAs@N-TC and Ru-SAs@N-TC. Reproduced with permission from Ref. [85], © WILEY-VCH Verlag GmbH & Co. KGaA, Weinheim 2020.

friendly. Most of these catalysts can retain the characteristic structure of pristine MOFs extremely. Herein, a summary of the performance of Ru-doped other MOF derivatives toward EWS is shown in Table 4.

**Defective MOFs.** Generally, thermal treatment is the most common strategy for preparing defective MOFs, however, which will destroy unique pore structures. To solve this issue, the defective MOFs with the original characteristic morphology have been reported by some mild methods. For instance, Liu and co-workers reported the ultra-low Ru doped defective CoFe-MOF (Ru@CoFe/D-MOF) hollow nanorods via the NaBH<sub>4</sub> reduction at ambient temperature, and the formation of hollow structure was based on the Kirkendall effect (Fig. 12(a)) [108]. The formation of oxygen vacancy ( $O_v$ ) defects is described in Fig. 12(b). Benefiting from the synergistic effect of Ru active sites, CoFe nanoparticles, and structural defects, the overpotential of the well-designed Ru@CoFe/D-MOF-2 decreased significantly compared to the pristine Co-MOF, with 242 mV at 10 mA·cm<sup>-2</sup>. Further, in order to explore the roles of  $O_v$  defects, the surface valence band spectra (VBS) noticed that the energy of d-band center ( $E_d$ ) positively shifted from CoFe-MOF and CoFe/D-MOF to Ru@CoFe/D-

MOF, respectively, indicating that the  $O_v$  defects could improve the intermediate adsorption on the catalysts (Fig. 12(c)). Overall, the partial reduction process provides abundant defects, which not only exposes more active sites, but also facilitates the loading of ultra-low Ru and further enhances the catalytic activity.

**MOF-derived metal hydroxides.** In recent years, metal hydroxides with intrinsic electrochemical activity are a kind of trend toward EWS. Liu and co-workers utilized *in situ* etching method to convert part of the pristine NiFe-MOF into active NiFe(OH)<sub>x</sub> (Figs. 12(d) and 12(e)) [109]. The calculated  $E_d$  of Ru/NiFe(OH)<sub>x</sub>/NiFe-MOF was found to be closer to 0 eV, suggesting that an intense adsorption was between electrochemical active sites and OER intermediates (OH<sup>•</sup>, OOH<sup>•</sup>, and O<sup>•</sup>). This etching strategy could not only lead to plentiful exposed defective regions to anchor Ru species, but also facilitate the binding of unsaturated metal sites with OH<sup>•</sup> ions, consequently improving the electron transfer efficiency and performance of OER. In addition, layered double hydroxide (LDH) materials have been paid increasing attention due to their outstanding OER activity [116, 117]. Hu's group prepared a MOF-derived amorphous/crystalline FeCoNi-LDH with atomically dispersed Ru

**Table 3** Electrocatalytic performance of MOF-derived metal oxides/sulfides/phosphides

Materials	Electrolytes	HER $\eta$ (mV@mA·cm <sup>-2</sup> )	OER $\eta$ (mV@mA·cm <sup>-2</sup> )	Tafel slope (mV·dec <sup>-1</sup> )	Stability (mA·cm <sup>-2</sup> ·h)	References
Cu-doped RuO <sub>2</sub>	0.5 M H <sub>2</sub> SO <sub>4</sub>	—	188@10	43.96	10@8 h	[96]
Zn-doped RuO <sub>2</sub>	0.5 M H <sub>2</sub> SO <sub>4</sub>	—	206@10	49	10@30 h	[97]
Cr <sub>0.6</sub> Ru <sub>0.4</sub> O <sub>2</sub>	0.5 M H <sub>2</sub> SO <sub>4</sub>	—	178@10	58	10@10 h	[98]
(Ru-Co)O <sub>x</sub>	1 M KOH	—	265@10	60	10@20 h	[99]
Hollow (Ru-Co)O <sub>x</sub>	1 M KOH	44.1@-10	171.2@10	23.5 (HER) 60.8 (OER)	10@10 h (OWS)	[100]
Ru-NiFeP/NF	0.5 M H <sub>2</sub> SO <sub>4</sub>	29@-10	179@10	67.8 (HER)	80 mV@24 h (HER)	[101]
	1 M PBS	105@-10	—	44.9 (OER)	1.45 V@20 h (OER)	
Cu-RuS <sub>2</sub> /Ru	1 M KOH	169@-200	—	70	-10@15 h	[102]
Ru-CoP NAs	1 M KOH	52@-10	—	39.7	-100@50 h	[103]

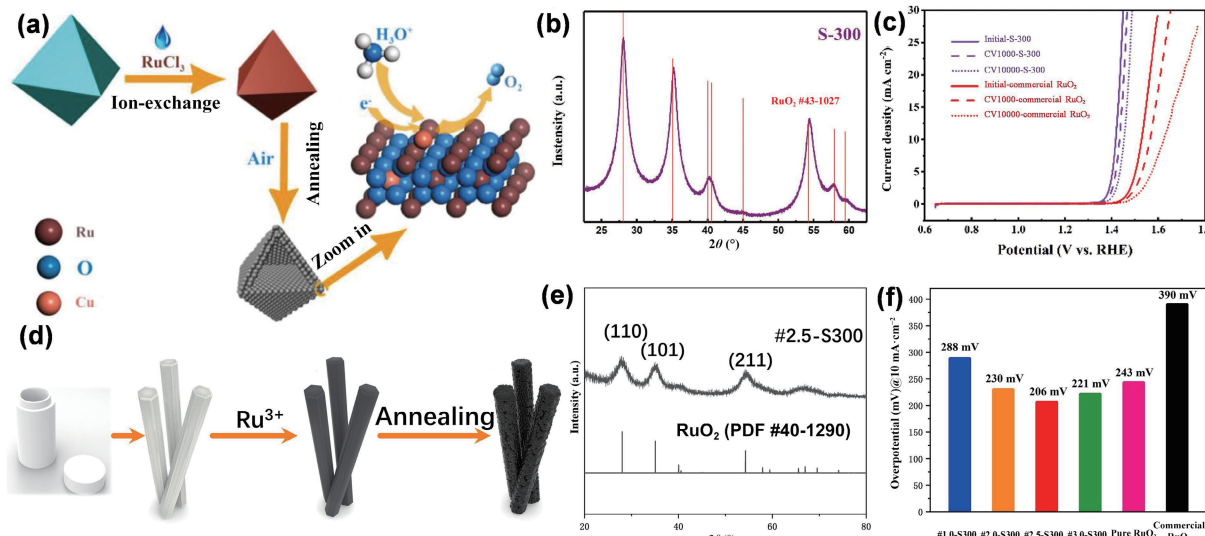


**Figure 10** (a) Synthetic route and model of Cu-doped RuO<sub>2</sub> hollow porous polyhedron. (b) XRD patterns of S-300. (c) Polarization curves of S-300 and commercial RuO<sub>2</sub>. Reproduced with permission from Ref. [96], © WILEY-VCH Verlag GmbH & Co. KGaA, Weinheim 2018. (d) Synthetic method and model of Zn-doped RuO<sub>2</sub>. (e) XRD patterns of #2.5-S300. (f) Overpotential@10mA·cm<sup>-2</sup> for Zn-doped RuO<sub>2</sub>, pure RuO<sub>2</sub>, and commercial RuO<sub>2</sub>. Reproduced with permission from Ref. [97], © Wiley-VCH GmbH 2020.

catalyst (Ru SAs/AC-FeCoNi) to enhance the OER performance [110]. Benefiting from the abundant defect sites, unsaturated coordination sites, and highly symmetric rigid structure, the Ru SAs/AC-FeCoNi catalyst performed remarkable activity and stability.

**Active substrates supported MOFs.** In addition, compounding with specific active carriers is also a rational method to enhance electrocatalytic performance [118]. For instance, Luo and co-workers fabricated ultrafine Ru nanoparticles from a composite of leaf-shaped ZIF-L(Co) MOF and polydopamine coated few-layered Ti<sub>3</sub>C<sub>2</sub>T<sub>x</sub> MXene (FL-Ti<sub>3</sub>C<sub>2</sub>T<sub>x</sub>) [111]. MXene was selected as a template to generate ZIF-L(Co) nanosheets and yet acted as a conductive support. The HRTEM image indicated that a large number of Ru nanoparticles (~ 4 nm) are uniformly dispersed on the carrier. And Ru@ZIF-L(Co)/FL-Ti<sub>3</sub>C<sub>2</sub>T<sub>x</sub> catalyst exhibited more activity and better electron transfer than pristine Ru@ZIF-L(Co). Generally speaking, the remarkable HER performance of the catalyst was a heterogeneous effect of the ZIF-L(Co) nanosheets with rich Ru active sites and the outstanding conductivity, great hydrophilicity, and high mechanical and electrochemical stability of MXene.

### 3 Ru-doped POPs and their derivatives

POPs are denoted to a series of 2D or three-dimensional (3D) network structures from organic groups or fragments by the

covalent linkages [119], such as COFs [120], covalent triazine skeletons (CTFs) [121], hyper-crosslinked polymers (HCPs) [122], conjugated microporous polymers (CMPs) [123], and polymers of intrinsic microporosity (PIMs) [124]. Based on the requirement of EWS for active sites and mass/electron transfer channels, metal-free POPs [125], metallized POPs [126, 127], metal-based materials incorporated in POPs [128], and POPs combined with conductive carbon materials [129] have been accordingly prepared. In special, the introduction of active Ru sites in POPs could effectively manipulate the electronic properties of the active sites by promoting the electron transfer process, and modulate the secondary environment around the catalytic active site to produce new electrochemical properties, further improving the electrocatalytic activity [130]. Hence, Ru-doped POPs and their derivatives have been paid increasing attention in recent years. Herein, a summary of the performance of Ru-doped POPs and their derivatives toward EWS is shown in Table 5.

#### 3.1 Ru-doped COFs and their derivatives

COFs have been reported as a new porous material for energy storage and conversion due to their well-defined pore structure and tunable porosity [138–140]. Similar to MOFs, COFs can provide the abundant anchoring sites for Ru active sites, facilitating electron and mass transfer. Specially, 2D-COFs exhibit higher specific surface area, relatively chemical stability, and have extraordinary electron transport properties due to the π-π



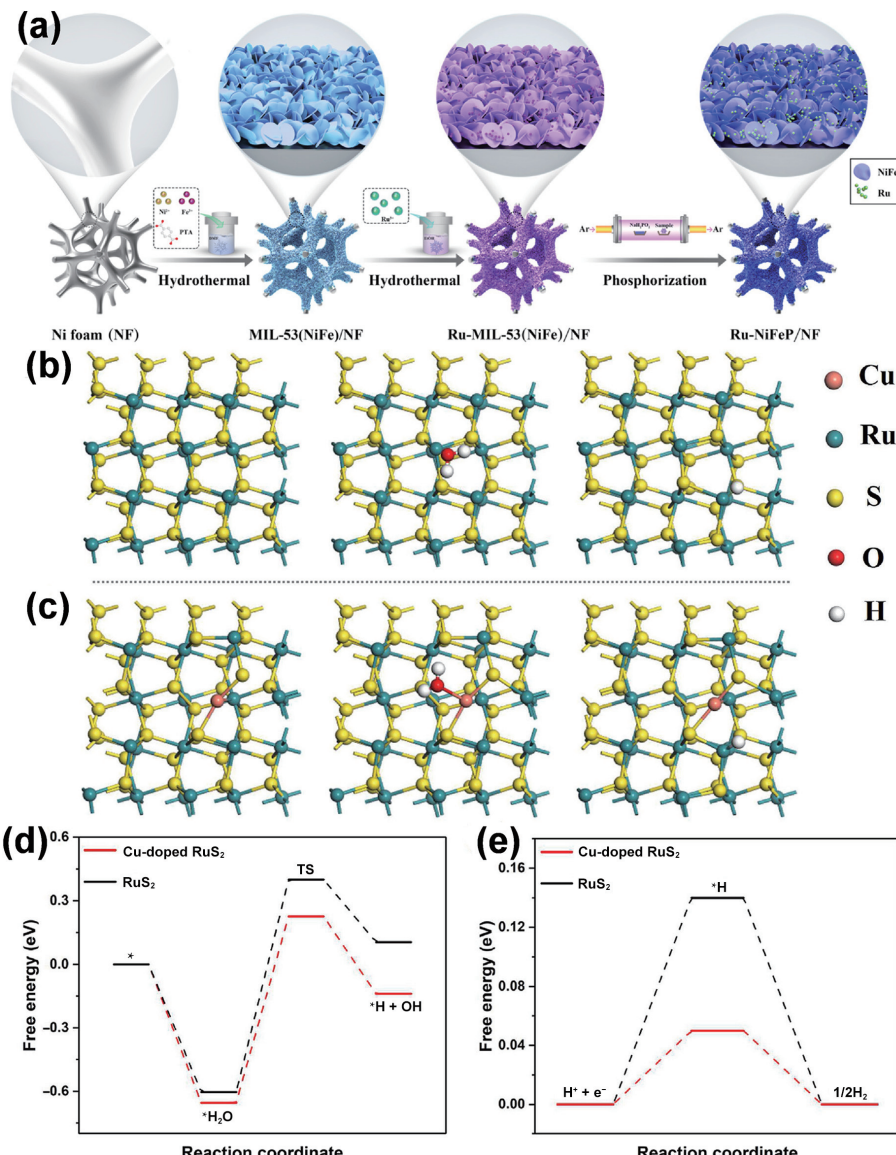


**Figure 11** (a) Synthesis of the Ru-NiFeP/NF nanosheets. Reproduced with permission from Ref. [101], © Elsevier B.V. 2020. (b) and (c) Theoretical structural models of clean surface and  $^*\text{H}_2\text{O}$ ,  $^*\text{H}$  intermediates adsorbed on the surfaces of  $\text{RuS}_2$  and Cu-doped  $\text{RuS}_2$ . (d) and (e) Calculated free energy diagram of water dissociation and H adsorption for Cu-doped  $\text{RuS}_2$  and  $\text{RuS}_2$ . Reproduced with permission from Ref. [102], © Elsevier Ltd. 2022.

interaction and the enhanced charge carrier mobility [141, 142]. By improving the intrinsic conductivity of 2D-COFs and combining with conductive substrates (e.g., reduced graphene oxide (rGO), carbon nanotubes (CNTs), and KB) and pyrolysis, series of Ru-doped 2D-COFs have been designed for EWS. Meanwhile, first-principles and DFT calculations have also confirmed the potential of 2D-COFs in EWS [143, 144].

Pan and co-workers prepared aromatic imide-based 2D-COF with high crystallinity via high temperature solvothermal method, and subsequently fabricated HER Cryst-2D-PMPI-Ru catalyst by loading Ru nanoclusters with special pore structure (Fig. 13(a)) [131]. TEM images noticed that Ru nanoclusters (~ 2 nm) were uniformly dispersed after carbonization (Fig. 13(b)), which was due to the great complexation capacity of polyimide with Ru<sup>3+</sup> ions and the uniform in-plane long range ordering of Cryst-2D-PMPI. Benefiting from the massive active sites provided by uniform and ultrasmall Ru nanoclusters, Cryst-2D-PMPI-Ru performed remarkable activity superior to commercial Pt/C (Fig. 13(c)). Moreover, the structure and composition were explored after the stability test, and there was mostly no change in XRD images, indicating the relatively good chemical stability of the structure. In brief, due to the homogeneous porosity, great complexation ability

with Ru<sup>3+</sup> ions, and the electrochemical stability of crystalline 2D-COF, small-sized Ru nanoclusters are homogeneously distributed in COF-derived 2D layered carbon, which exhibit remarkable HER performance in both acidic and alkaline electrolytes. Additionally, to further improve EWS performance, COFs can be combined with conductive carbon substrates through simple π-π stacking. Zhao and co-workers fabricated COF/rGO-Ru catalyst through multi-refluxing steps, in which COF was supported on the rGO, and subsequently Ru nanoparticles were embedded in the COF/rGO composite (Fig. 13(d)) [133]. From TEM image, it can be seen that Ru nanoparticles (1.2–2.8 nm) exhibited on the surface, indicating that Ru nanoparticles were successfully encapsulated inside the COF/rGO (Fig. 13(e)). Benefiting from the great conductive carrier and active Ru sites, the COF/rGO-Ru catalyst performed remarkable activity with an overpotential of 42 mV at 10 mA·cm<sup>-2</sup>, lower than the commercial Pt/C (Fig. 13(f)). In summary, the Ru-N moieties are successfully converted into Ru nanoparticles embedded in COF with conductive rGO by facile reflux process, consequently improving the EWS activities and stability. Meanwhile, 2D-COF can also be regarded as a rational nano-interlayer to separate adjacent graphene nano-layers and prevent the stacking of graphene, thereby enhancing mass

**Table 4** Electrocatalytic performance of Ru-doped other MOF derivatives

Materials	Electrolytes	HER $\eta$ (mV@mA·cm <sup>-2</sup> )	OER $\eta$ (mV@mA·cm <sup>-2</sup> )	Tafel slope (mV·dec <sup>-1</sup> )	Stability (mA·cm <sup>-2</sup> @h)	References
Ru@p-Co <sub>3</sub> HHTP <sub>2</sub>	1 M KOH	19@–10	—	42	–100@25 h	[107]
	0.5 M H <sub>2</sub> SO <sub>4</sub>	35@–10	—	21	–10@12 h	[107]
	1 M PBS	50@–10	—	33	–10@12 h	[107]
Ru@CoFe/D-MOF	1 M KOH	—	265@10	47.66	10@40 h	[108]
Ru/NiFe(OH) <sub>x</sub> /NiFe-MOF	1 M KOH	—	242@10	30.63	10@36 h	[109]
Ru SAs/AC-FeCoNi	1 M KOH	—	205@10	40	10@48 h	[110]
Ru@ZIF-L(Co)/FL-Ti <sub>3</sub> C <sub>2</sub> T <sub>x</sub>	1 M KOH	16.2@–10	—	21	–10@10 h	[111]
MXene@RuCo NPs	1 M KOH	20@–10	253@10	30.4 (HER) 61.3 (OER)	–100@18 h (HER) 100@18 h (OER)	[112]

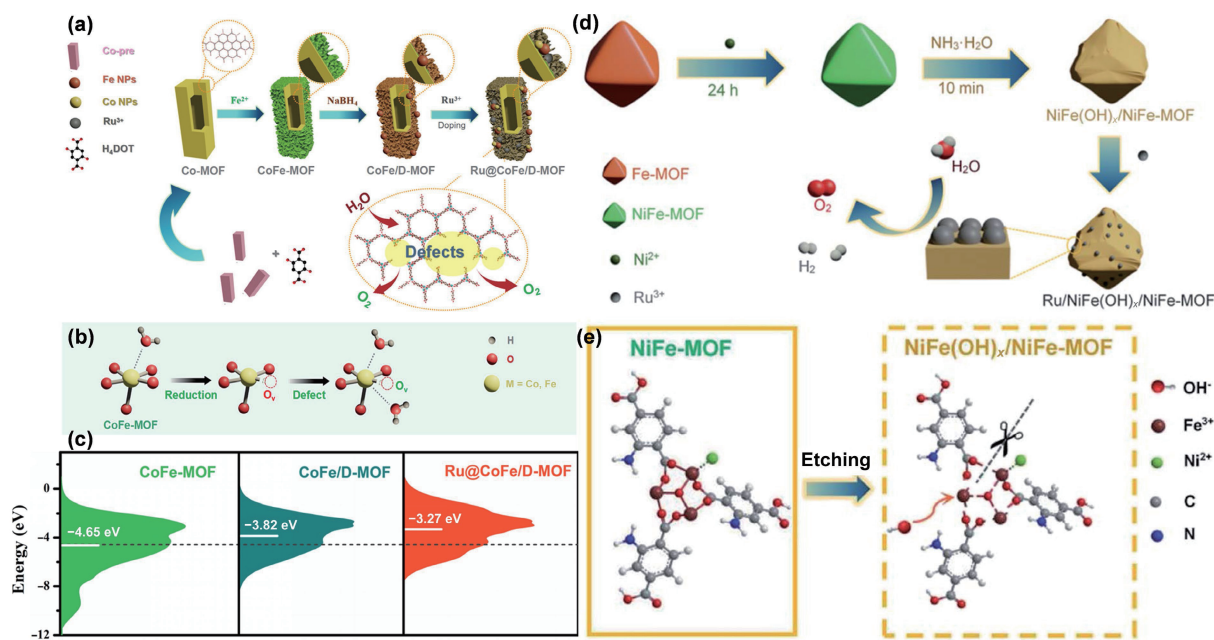


**Figure 12** (a) Synthesis of Ru@CoFe/D-MOF electrocatalyst. (b) Mechanism for the formation of defects within the MOF structure. (c) Surface valence band spectra of Ru@CoFe/D-MOFs. Reproduced with permission from Ref. [108], © the Partner Organisations 2022. (d) Synthetic route of Ru/NiFe(OH)<sub>x</sub>/NiFe-MOF electrocatalyst. (e) Scheme of the structure of NiFe-MOF and the formation process of NiFe(OH)<sub>x</sub>/NiFe-MOF during the etching process. Reproduced with permission from Ref. [109], © The Royal Society of Chemistry 2021.

transport and the accessibility of the Ru-N parts.

In 2016, Zhang's group firstly reported 2D-COFs with fully sp<sup>2</sup>-bonded carbon skeleton, which was more stable than mainstream imine-based COFs [145]. Recently, COFs through sp<sup>2</sup> carbon-carbon double bond connection have been paid much attention due to the facilitated stability and improved  $\pi$ -delocalization. Zhao and co-workers prepared a novel catalyst (Ru@COF-1) by complexation of triazine-cored sp<sup>2</sup> carbon-conjugated COF with Ru ions (Fig. 14(a)) [134]. In order to confirm coordination of the triazine moieties of COF-1 with Ru ions, XPS was accordingly tested. It obviously can be seen that the catalyst exhibited a new characteristic peak at 399.4 eV, corresponding to a portion of the N coordinated with the Ru ions, indicating that Ru ions were successfully coordinated with COF-1 (Fig. 14(b)). Moreover, Ru@COF-1 performed efficient activity in acidic solutions, with an overpotential of 200 mV at 10 mA·cm<sup>-2</sup>. And HER activity did not deteriorate after 1000 cyclic voltammetry (CV) cycles. The reason was found that triazine moieties would protonate in the acidic environment (Figs. 14(c) and 14(d)), which could improve the conductivity of COFs (Fig. 14(e)), consequently enhancing the electrocatalytic performance. In brief, the outstanding performance might be attributed to the crucial factors: The sp<sup>2</sup> carbon conjugated COF-1 as a matrix can maintain crystallinity in acidic medium and generate steady coordination structure between COF and Ru species.

### 3.2 Ru-doped CTFs and their derivatives

In 2008, series of polymers with triazine linkages were synthesized by high dynamic condensation reaction, and the concept of CTFs was proposed for the first time [146]. Their special porous structure and electronic properties provide a favorable carbon carrier for catalysts [147]. Considering that the interface effect between Ru-based catalysts and carbon substrate could enhance EWS performance, it is essential to design Ru-doped CTFs and their derivatives and explore structure–activity relationships.

Gao and co-workers rationally prepared the defect covalent triazine frameworks (D-CTFs) carrier and fabricated Ru/D-CTFs-900 composite subsequently through a facile one-pot pyrolysis (Fig. 15(a)) [135]. And the OER catalyst Ru-RuO<sub>2</sub>-CTFs-300 was obtained by calcined in the air. Thanks to the abundant defective areas, highly dispersed Ru nanoparticles were anchored on the substrate. In the HRTEM images, 0.205, 0.318, and 0.225 nm lattice fringe spacings were distinctly observed (Figs. 15(b) and 15(c)), which were attributed to the (101) crystal plane of the hcp Ru, and the (110) and (101) crystal facet of the RuO<sub>2</sub>, respectively. Based on the great HER/OER activity, an overall water splitting device with two-electrode configuration was fabricated, which applied only 1.47 V at 10 mA·cm<sup>-2</sup>, 20% better than Pt/C//RuO<sub>2</sub>/C (Fig. 15(d)). Furthermore, the DFT calculations were carried out to gain more insight into the EWS activity. Ru<sub>38</sub>/N and Ru<sub>38</sub>O<sub>7</sub>/N were taken to simulate the catalyst in the cathode (Ru/D-CTFs-

**Table 5** Electrocatalytic performance of Ru-doped POPs and their derivatives

Materials	Electrolytes	HER $\eta$ (mV@mA·cm <sup>-2</sup> )	OER $\eta$ (mV@mA·cm <sup>-2</sup> )	Tafel slope (mV·dec <sup>-1</sup> )	Stability (mA·cm <sup>-2</sup> @h)	References
Cryst-2D-PMPI-Ru	1 M KOH	35.1@-10	—	36.5	—	[131]
	0.5 M H <sub>2</sub> SO <sub>4</sub>	55.3@-10	—	31.3	—	
Ru@2D COF	1.5 M H <sub>2</sub> SO <sub>4</sub>	159@-10	—	79	—	[132]
	1 M KOH	42@-10	—	46	-10@20 h (KOH)	[133]
COF/rGO-Ru	0.5 M H <sub>2</sub> SO <sub>4</sub>	132@-10	—	—	—	[133]
	0.5 M H <sub>2</sub> SO <sub>4</sub>	200@-10	—	140	—	[134]
Ru@COF-1	0.5 M H <sub>2</sub> SO <sub>4</sub>	200@-10	—	—	—	[135]
Ru/D-CTFs-900	1 M KOH	17@-10	—	32	1.12 V@20 h	[135]
Ru-RuO <sub>2</sub> /D-CTFs	1 M KOH	—	190@10	41	1.47 V@20 h	[135]
HCP-PPh <sub>3</sub> -Ru	1 M KOH	61@-10	—	73	—	[136]
Ru@Bpy-POP	1 M KOH	—	270@10	67	1.57 V@24 h	[130]
Ru/NPCS	0.5 M H <sub>2</sub> SO <sub>4</sub>	14.4@-10	—	35	500@120 h (MEA)	[137]

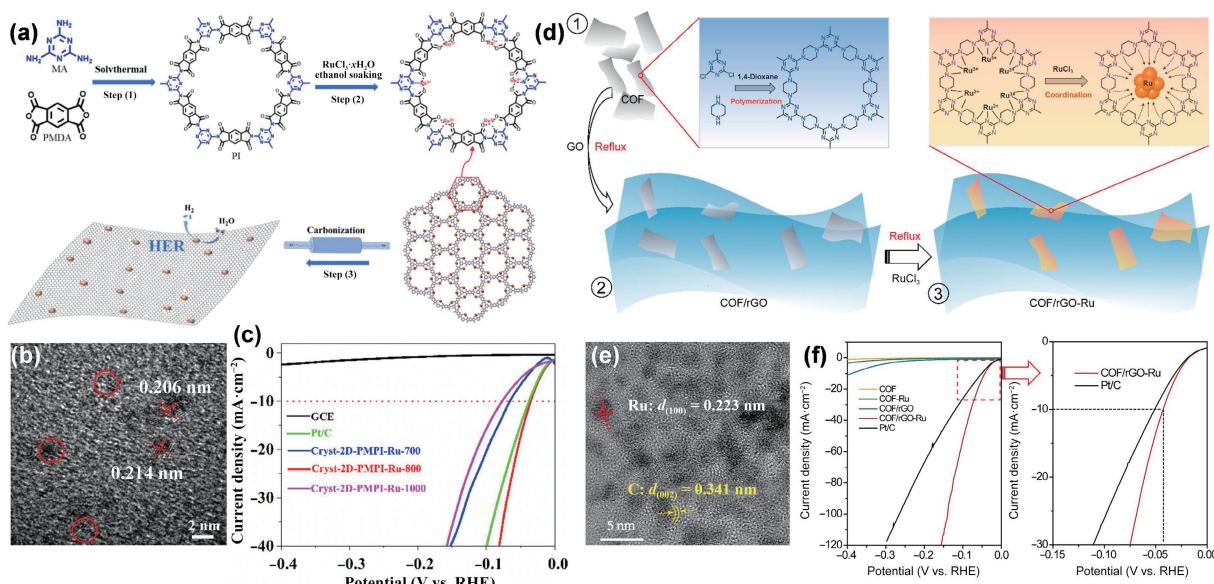


**Figure 13** (a) Synthetic route of the method of Cryst-2D-PMPI. (b) TEM image of Cryst-2D-PMPI-Ru. (c) Polarization curves of series of Cryst-2D-PMPI-Ru in 1 M KOH. Reproduced with permission from Ref. [131], © Elsevier B.V. 2021. (d) Preparation procedure of COF/rGO-Ru. (e) TEM image of COF/rGO-Ru. (f) Polarization curves of series COF hybrids. Reproduced with permission from Ref. [133], © American Chemical Society 2021.

900) and in the anode (Ru-RuO<sub>2</sub>-CTFs-300), respectively (Fig. 15(e)). Comparing upper site and lower site of the  $\Delta G$  curve of the elemental steps, it was found that the high covalent nature of the Ru–O bond reduced the interaction between adjacent Ru and O atoms in the OER species and promoted excellent performance (Figs. 15(f) and 15(g)). In addition, the HER reaction steps were also calculated and displayed in Fig. 15(h), indicating that the introduction of Ru ions efficiently weakened the adsorption of hydrogen atoms and consequently enhanced the HER activity.

### 3.3 Ru-doped HCPs and their derivatives

In the early 1970s, HCPs were initially reported by Davankov's group [148]. The synthesis of HCPs is mainly based on Friedel–Crafts chemistry, which provides fast kinetics to form strong linkages, resulting in a highly crosslinked microporous network with remarkable porosity [149]. Recently, microporous polymers have attracted considerable attention due to their outstanding properties such as high specific surface area, plentiful functional groups, and good chemical and thermal stability. In view of this, it is promising to explore the Ru-doped HCPs and their derivatives as EWS catalysts.

Xu and co-workers reported the coordination of Ru catalyst in the interior space of the HCP-PPh<sub>3</sub> synthesized through cross-linking of PPh<sub>3</sub> and benzene (Fig. 16(a)) [136]. As shown in Fig. 16(b), elements C, P, and Ru were randomly dispersed in HCP-

PPh<sub>3</sub>-Ru(III) (5.0 wt.%), verifying the successful fabrication. And there were not notable changes in the Fourier-transform infrared (FT-IR) spectrum of HCP-PPh<sub>3</sub>-Ru(III) (5.0 wt.%), suggesting that the framework of HCP-PPh<sub>3</sub> could not been affected after loading Ru(III) (Fig. 16(c)). Moreover, the catalyst exhibited relatively good HER performance, with a 61 mV overpotential at 10 mA·cm<sup>-2</sup> (Fig. 16(d)). And it can be evidently seen that there was no degradation of the overpotential after 1000 CV cycles, suggesting the relatively high stability (Fig. 16(e)). Besides, EIS experiments noticed that catalyst displayed smallest charge transfer resistance ( $R_{ct}$ ), indicating more facile electrode kinetic (Fig. 16(f)). In summary, the high HER activity and durability of the catalyst might be ascribed to the following factors: (1) The high porosity and unique pore structure of HCP-PPh<sub>3</sub> are beneficial to the stability and distribution of Ru nanoparticles. (2) The P-functional groups can promote the anchoring of Ru as a coordination point to stabilize small-sized Ru nanoparticles, hence improving the HER activity.

## 4 Conclusions and perspectives

Electrocatalytic water splitting is considered to be one of the most promising methods for producing hydrogen energy, yet the state-of-the-art precious metal (Pt/Ir)-based EWS catalysts still face a series of problems. As the most effective substitute for the Pt/Ir-

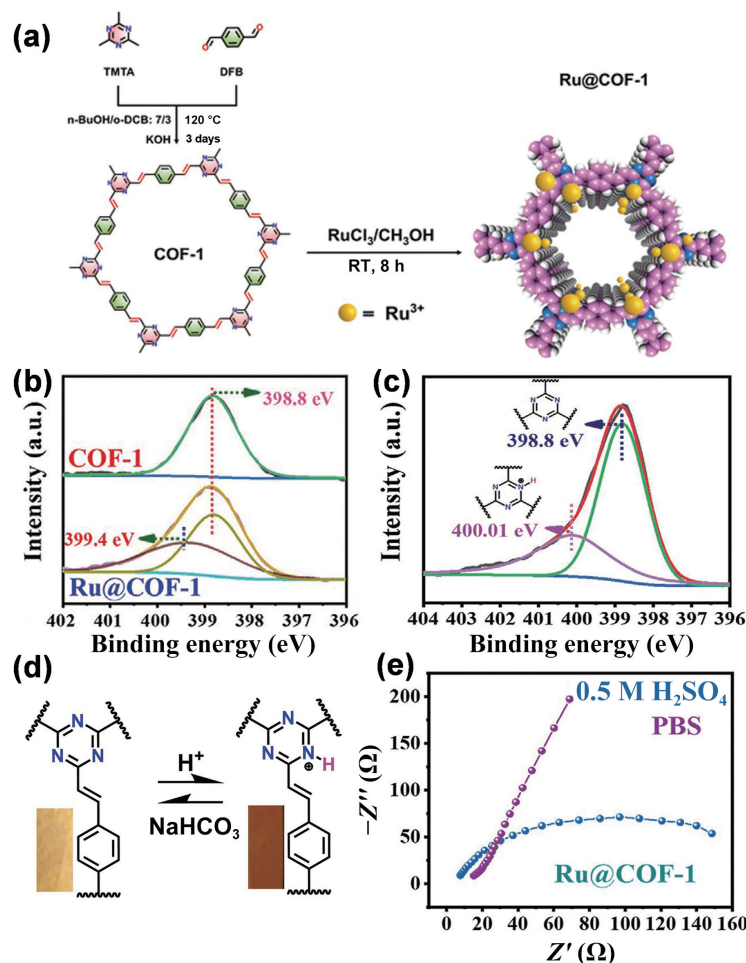


**Figure 14** (a) Syntheses of COF-1 and Ru@COF-1. (b) N 1s XPS spectra of COF-1 and Ru@COF-1. (c) N 1s XPS spectra of Ru@COF-1 in acidic solutions. (d) Structure and color of COF-1 in acid and base solutions. (e) EIS Nyquist plots of Ru@COF-1. Reproduced with permission from Ref. [134], © Wiley-VCH GmbH 2022.

based catalysts, Ru-based nanomaterials have aroused much attention in recent years. In particular, the emerging of the functional porous materials, including MOFs and POPs, offers good platform for the tuning of Ru-based active site towards EWS. And the advantages of these Ru doped functional porous materials are as follows: (1) The defect of pristine functional porous materials can be produced by tuning the absence of metal nodes, which is conducive to the anchoring of Ru species, subsequently improving the durability of the catalyst. (2) The well-defined porous structure of functional porous materials is beneficial to the mass transport in the catalytic process. (3) The metal centers and heteroatoms of functional porous materials can optimize the electronic configuration of Ru sites and synergistically enhance their catalytic performance.

In this review, the design, preparation strategies, and structure–activity relationship exploration of the Ru-doped functional porous materials toward EWS are comprehensively summarized, including Ru-doped MOFs, Ru-doped POPs, and their derivatives. Among them, researches on Ru-doped MOFs and their derivatives are the most extensive, due to the abundant metal/ligand nodes, porous structure, and high surface area of MOFs. Atomic Ru sites, Ru nanoparticles, and Ru-based alloys can be successfully doped into the pristine MOFs, which brings about the optimization of electronic structure of Ru active sites, as well as their adsorption energy for H<sub>2</sub>O and the key intermediates. To further avoid the disadvantages of pristine MOFs in electronic conductivity and stability, reduction strategy, introducing active carriers, and partially etching of MOFs have been seen as the effective methods for the Ru-doped MOFs materials. On the other

hand, pyrolysis under different gases (N<sub>2</sub>, air, NH<sub>3</sub>, etc.) can also be used to solve the these low-conductivity/stability problems. And series of Ru-doped MOF derivatives such as Ru-doped carbon-based materials and Ru-doped metal oxides/sulfides/phosphides are accordingly developed, most of which have achieved excellent EWS performance at industrial current densities. In addition, Ru-doped POPs and their derivatives (COFs, CTFs, HCPs, etc.) have been paid increasing attention due to their well-defined pore structure and tunable porosity, which are huge potential to improve the EWS performance.

Despite the promising prospect for the EWS process with the rapid development of Ru-doped functional porous materials, several challenges for the field are still available, which need to be recognized and solved in the future. Details are as follows:

(1) Stability. Up to date, Ru-doped functional porous materials still own limited stability due to inevitable characteristics of the Ru and MOFs species, even though much researches have been focused on this topic. The stability of the inner loaded Ru species can be improved due to the protection of porous functional materials. Yet the exposed Ru/RuO<sub>2</sub> species on the surface are easily removed or overoxidized into soluble RuO<sub>4</sub> under harsh electrochemical environment, which leads to the poor OER stability. As for the MOFs carriers, the metal nodes and organic ligands are easily destroyed under the EWS conditions, which would bring confusion to the research on the EWS catalytic mechanism.

(2) Conductivity. The low conductivity of Ru-doped functional porous materials is the key bottlenecks for their development in the EWS area. So far, pyrolytic transformation and coupling with

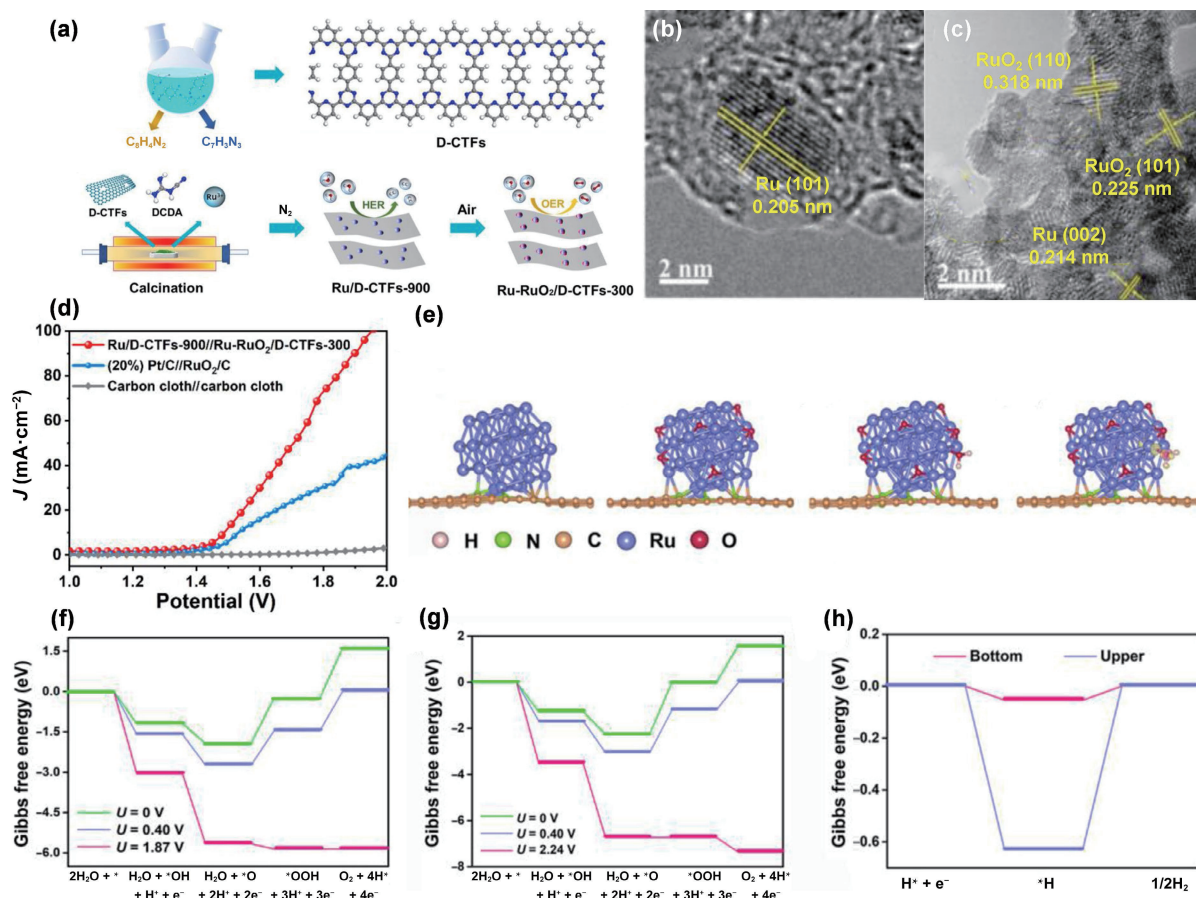


**Figure 15** (a) Synthesis of D-CTFs, Ru/D-CTFs, and Ru-RuO<sub>2</sub>/D-CTFs. (b) HRTEM images of Ru/D-CTFs-900 and (c) Ru-RuO<sub>2</sub>/D-CTFs-300. (d) Polarization curves of two-electrode configuration in 1 M KOH. (e) Optimal structure of Ru<sub>38</sub>/N-PC, Ru<sub>38</sub>O<sub>7</sub>/N-PC, H<sub>2</sub>O adsorption on the upper site of Ru<sub>38</sub>/N-PC, and corresponding distribution of transferred charges, left to right, respectively. (f) Upper site of Ru<sub>38</sub>O<sub>7</sub>/N-PC and (g) bottom site of Ru<sub>38</sub>O<sub>7</sub>/N-PC. (h) Free energy scheme of HER on Ru<sub>38</sub>/N-PC. Reproduced with permission from Ref. [135], © Science Press and Dalian Institute of Chemical Physics, Chinese Academy of Sciences. Published by Elsevier B.V. and Science Press 2020.

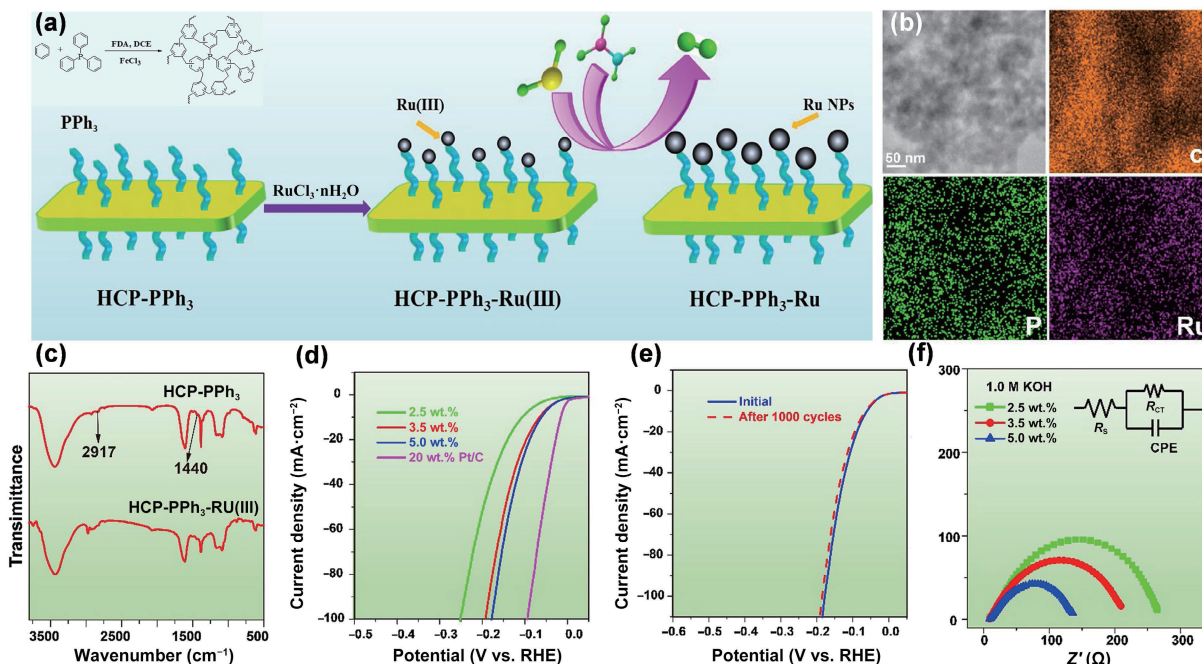


**Figure 16** (a) Synthetic route of HCP-PPPh<sub>3</sub> and HCP-PPPh<sub>3</sub>-Ru. (b) STEM energy dispersive X-ray spectroscopy (EDS) images of HCP-PPPh<sub>3</sub>-Ru(III) (5.0 wt.%). (c) FT-IR spectrum of HCP-PPPh<sub>3</sub>-Ru(III). (d) Polarization curves for series of HCP-PPPh<sub>3</sub>-Ru and 20 wt.% Pt/C for HER. (e) Polarization curves for HCP-PPPh<sub>3</sub>-Ru (5.0 wt.%) before and after 1000 CV cycles. (f) EIS Nyquist plots of the as-prepared catalysts in 1 M KOH. Reproduced with permission from Ref. [136], © Elsevier B.V. 2018.

conductive substrate are most available strategies to improve their conductivity, yet multi-steps process will be inevitably undergone and the structural advantages of MOFs are hard to be maintained.

Hence, from the perspective of synthetic strategy optimization, developing conductive functional porous materials is also an effective way to solve this problem.

(3) Ambiguous EWS mechanism. Although the electronic configuration and coordination environment of Ru-doped functional porous materials have been studied by some advanced characterization techniques, such as *operando* X-ray absorption fine structure (XAFS) and DFT calculations, the real active sites and metal-support interaction of Ru-doped functional porous materials are still lack of in-depth discussion. Therefore, it is necessary to develop more *in situ/operando* characterization techniques for the mechanism research on the EWS process.

(4) The mass creation of novel functional porous materials for EWS. Most of the reported porous functional materials for EWS are MOFs dominated materials such as ZIF-67, ZIF-8, MIL-101, and UIO-66. MOFs with novel metal-ligand coordination need to be explored to improve the EWS performance. At the same time, other functional frameworks such as COFs and hydrogen-bonded organic frameworks (HOFs) also exhibit potential for EWS due to their unique coordination configuration, yet lack of thorough exploration. Besides, it is urgently needed for large-scale production of those functional porous materials to meet their application in the industrial EWS devices.

(5) Industrial scale applications. The cost is the most important factor to realize industrial production. In order to reduce the cost of Ru-doped functional porous materials, the following points can be considered: (a) optimizing the harsh synthesis conditions; (b) designing self-supporting catalysts to reduce the amount of Nafion binder; (c) reducing the Ru loading and improve their intrinsic properties; and (d) neutral medium could be preferred as electrolyte.

Overall, Ru-doped functional porous materials have performed excellent HER and OER performance, and some reported catalysts have achieved overall water splitting under industrial current. In spite of the problems existed in Ru-doped functional porous materials, the unique compositional and structural advantages of the Ru species and functional porous materials still bring the broad prospect in the field of EWS.

## Acknowledgements

This work was financially supported by the National Key Research and Development Program of China (No. 2020YFB1506300), the National Natural Science Foundation of China (Nos. 21971017, 21922502, and 22075018), Young Elite Scientists Sponsorship Program by BAST (No. BYESS2023163), CNPC Innovation Found (No. 2022DQ02-0606), and Beijing Institute of Technology Research Fund Program.

## References

- [1] Dresselhaus, M. S.; Thomas, I. L. Alternative energy technologies. *Nature* **2001**, *414*, 332–337.
- [2] Zou, X. X.; Zhang, Y. Noble metal-free hydrogen evolution catalysts for water splitting. *Chem. Soc. Rev.* **2015**, *44*, 5148–5180.
- [3] Zhang, C. H.; Guo, Z. W.; Tian, Y.; Yu, C. M.; Liu, K. S.; Jiang, L. Engineering electrode wettability to enhance mass transfer in hydrogen evolution reaction. *Nano Res. Energy* **2023**, *2*, e9120063.
- [4] Zhang, K. X.; Liang, X.; Wang, L. N.; Sun, K.; Wang, Y. N.; Xie, Z. B.; Wu, Q. N.; Bai, X. Y.; Hamdy, M. S.; Chen, H. et al. Status and perspectives of key materials for PEM electrolyzer. *Nano Res. Energy* **2022**, *1*, e9120032.
- [5] Han, L.; Dong, S. J.; Wang, E. K. Transition-metal (Co, Ni, and Fe)-based electrocatalysts for the water oxidation reaction. *Adv. Mater.* **2016**, *28*, 9266–9291.
- [6] Li, Y. J.; Sun, Y. J.; Qin, Y. N.; Zhang, W. Y.; Wang, L.; Luo, M. C.; Yang, H.; Guo, S. J. Recent advances on water-splitting electrocatalysis mediated by noble-metal-based nanostructured materials. *Adv. Energy Mater.* **2020**, *10*, 1903120.
- [7] Zeng, L. Y.; Zhao, Z. L.; Lv, F.; Xia, Z. H.; Lu, S. Y.; Li, J.; Sun, K. A.; Wang, K.; Sun, Y. J.; Huang, Q. Z. et al. Anti-dissolution Pt single site with Pt(OH)(O<sub>3</sub>)/Co(P) coordination for efficient alkaline water splitting electrolyzer. *Nat. Commun.* **2022**, *13*, 3822.
- [8] Wang, J.; Ji, Y. J.; Yin, R. G.; Li, Y. Y.; Shao, Q.; Huang, X. Q. Transition metal-doped ultrathin RuO<sub>2</sub> networked nanowires for efficient overall water splitting across a broad pH range. *J. Mater. Chem. A* **2019**, *7*, 6411–6416.
- [9] Zhu, Y. L.; Tahini, H. A.; Hu, Z. W.; Dai, J.; Chen, Y. B.; Sun, H. N.; Zhou, W.; Liu, M. L.; Smith, S. C.; Wang, H. T. et al. Unusual synergistic effect in layered ruddlesden-popper oxide enables ultrafast hydrogen evolution. *Nat. Commun.* **2019**, *10*, 149.
- [10] Wu, Z. Y.; Chen, F. Y.; Li, B. Y.; Yu, S. W.; Finfrock, Y. Z.; Meira, D. M.; Yan, Q. Q.; Zhu, P.; Chen, M. X.; Song, T. W. et al. Non-iridium-based electrocatalyst for durable acidic oxygen evolution reaction in proton exchange membrane water electrolysis. *Nat. Mater.* **2022**, *22*, 100–108.
- [11] Li, L. G.; Wang, P. T.; Shao, Q.; Huang, X. Q. Recent progress in advanced electrocatalyst design for acidic oxygen evolution reaction. *Adv. Mater.* **2021**, *33*, 2004243.
- [12] Rong, C. L.; Shen, X. J.; Wang, Y.; Thomsen, L.; Zhao, T. W.; Li, Y. B.; Lu, X. Y.; Amal, R.; Zhao, C. Electronic structure engineering of single-atom Ru sites via Co-N<sub>4</sub> sites for bifunctional pH-universal water splitting. *Adv. Mater.* **2022**, *34*, 2110103.
- [13] Wang, Y.; Pan, Y.; Zhu, L. K.; Yu, H. H.; Duan, B. Y.; Wang, R. W.; Zhang, Z. T.; Qiu, S. L. Solvent-free assembly of Co/Fe-containing MOFs derived N-doped mesoporous carbon nanosheets for ORR and HER. *Carbon* **2019**, *146*, 671–679.
- [14] Ding, J. Y.; Yang, H.; Zhang, S. S.; Liu, Q.; Cao, H. Q.; Luo, J.; Liu, X. J. Advances in the electrocatalytic hydrogen evolution reaction by metal nanoclusters-based materials. *Small* **2022**, *18*, 2204524.
- [15] Bao, F. X.; Yang, Z. L.; Yuan, Y. L.; Yu, P. L.; Zeng, G. M.; Cheng, Y.; Lu, Y. F.; Zhang, J. W.; Huang, H. W. Synergistic cascade hydrogen evolution boosting via integrating surface oxophilicity modification with carbon layer confinement. *Adv. Funct. Mater.* **2022**, *32*, 2108991.
- [16] Kweon, D. H.; Okyay, M. S.; Kim, S. J.; Jeon, J. P.; Noh, H. J.; Park, N.; Mahmood, J.; Baek, J. B. Ruthenium anchored on carbon nanotube electrocatalyst for hydrogen production with enhanced Faradaic efficiency. *Nat. Commun.* **2020**, *11*, 1278.
- [17] Liu, J. L.; Zheng, Y.; Zhu, D. D.; Vasileff, A.; Ling, T.; Qiao, S. Z. Identification of pH-dependent synergy on Ru/MoS<sub>2</sub> interface: A comparison of alkaline and acidic hydrogen evolution. *Nanoscale* **2017**, *9*, 16616–16621.
- [18] Luo, T. M.; Huang, J. F.; Hu, Y. Z.; Yuan, C. K.; Chen, J. S.; Cao, L. Y.; Kajiyoshi, K.; Liu, Y. J.; Zhao, Y.; Li, Z. J. et al. Fullerene lattice-confined Ru nanoparticles and single atoms synergistically boost electrocatalytic hydrogen evolution reaction. *Adv. Funct. Mater.* **2023**, *33*, 2213058.
- [19] Ma, X. F.; Xiao, H.; Gao, Y.; Zhao, M.; Zhang, L.; Zhang, J. M.; Jia, J. F.; Wu, H. S. Enhancement of pore confinement caused by the mosaic structure on Ru nanoparticles for pH-universal hydrogen evolution reaction. *J. Mater. Chem. A* **2023**, *11*, 3524–3534.
- [20] Su, P. P.; Pei, W.; Wang, X. W.; Ma, Y. F.; Jiang, Q. K.; Liang, J.; Zhou, S.; Zhao, J. J.; Liu, J.; Lu, G. Q. Exceptional electrochemical HER performance with enhanced electron transfer between Ru nanoparticles and single atoms dispersed on a carbon substrate. *Angew. Chem., Int. Ed.* **2021**, *60*, 16044–16050.
- [21] Wang, J.; Wei, Z. Z.; Mao, S. J.; Li, H. R.; Wang, Y. Highly uniform Ru nanoparticles over N-doped carbon: pH and temperature-universal hydrogen release from water reduction. *Energy Environ. Sci.* **2018**, *11*, 800–806.
- [22] Wu, Y. L.; Li, X. F.; Wei, Y. S.; Fu, Z. M.; Wei, W. B.; Wu, X. T.; Zhu, Q. L.; Xu, Q. Ordered macroporous superstructure of nitrogen-doped nanoporous carbon implanted with ultrafine Ru nanoclusters for efficient pH-universal hydrogen evolution reaction. *Adv. Mater.* **2021**, *33*, 2006965.
- [23] Yang, W. X.; Zhang, W. Y.; Liu, R.; Lv, F.; Chao, Y. G.; Wang, Z. C.; Guo, S. J. Amorphous Ru nanoclusters onto Co-doped 1D carbon nanocages enables efficient hydrogen evolution catalysis. *Chin. J. Catal.* **2022**, *43*, 110–115.



- [24] Du, J.; Li, F.; Sun, L. C. Metal-organic frameworks and their derivatives as electrocatalysts for the oxygen evolution reaction. *Chem. Soc. Rev.* **2021**, *50*, 2663–2695.
- [25] Li, C.; Zhang, H.; Liu, M.; Lang, F. F.; Pang, J. D.; Bu, X. H. Recent progress in metal-organic frameworks (MOFs) for electrocatalysis. *Ind. Chem. Mater.* **2023**, *1*, 9–38.
- [26] Li, Y.; Karimi, M.; Gong, Y. N.; Dai, N.; Safarifard, V.; Jiang, H. L. Integration of metal-organic frameworks and covalent organic frameworks: Design, synthesis, and applications. *Matter* **2021**, *4*, 2230–2265.
- [27] Wang, X. L.; Dong, L. Z.; Qiao, M.; Tang, Y. J.; Liu, J.; Li, Y. F.; Li, S. L.; Su, J. X.; Lan, Y. Q. Exploring the performance improvement of the oxygen evolution reaction in a stable bimetal-organic framework system. *Angew. Chem., Int. Ed.* **2018**, *57*, 9660–9664.
- [28] Yang, D. H.; Tao, Y.; Ding, X. S.; Han, B. H. Porous organic polymers for electrocatalysis. *Chem. Soc. Rev.* **2022**, *51*, 761–791.
- [29] Yu, J. H.; Corma, A.; Li, Y. Functional porous materials chemistry. *Adv. Mater.* **2020**, *32*, 2006277.
- [30] Bae, S. Y.; Mahmood, J.; Jeon, I. Y.; Baek, J. B. Recent advances in ruthenium-based electrocatalysts for the hydrogen evolution reaction. *Nanoscale Horiz.* **2020**, *5*, 43–56.
- [31] Han, S. M.; Yun, Q. B.; Tu, S. Y.; Zhu, L. J.; Cao, W. B.; Lu, Q. P. Metallic ruthenium-based nanomaterials for electrocatalytic and photocatalytic hydrogen evolution. *J. Mater. Chem. A* **2019**, *7*, 24691–24714.
- [32] Yang, Y. J.; Yu, Y. H.; Li, J.; Chen, Q. R.; Du, Y. L.; Rao, P.; Li, R. S.; Jia, C. M.; Kang, Z. Y.; Deng, P. L. et al. Engineering ruthenium-based electrocatalysts for effective hydrogen evolution reaction. *Nano-Micro Lett.* **2021**, *13*, 160.
- [33] Yu, J.; He, Q. J.; Yang, G. M.; Zhou, W.; Shao, Z. P.; Ni, M. Recent advances and prospective in ruthenium-based materials for electrochemical water splitting. *ACS Catal.* **2019**, *9*, 9973–10011.
- [34] Zhu, J. T.; Cai, L. J.; Tu, Y. D.; Zhang, L. F.; Zhang, W. J. Emerging ruthenium single-atom catalysts for the electrocatalytic hydrogen evolution reaction. *J. Mater. Chem. A* **2022**, *10*, 15370–15389.
- [35] Furukawa, H.; Cordova, K. E.; O’Keeffe, M.; Yaghi, O. M. The chemistry and applications of metal-organic frameworks. *Science* **2013**, *341*, e1230444.
- [36] Yaghi, O. M.; Li, G. M.; Li, H. L. Selective binding and removal of guests in a microporous metal-organic framework. *Nature* **1995**, *378*, 703–706.
- [37] Wang, Q.; Astruc, D. State of the art and prospects in metal-organic framework (MOF)-based and MOF-derived nanocatalysis. *Chem. Rev.* **2020**, *120*, 1438–1511.
- [38] Li, C. F.; Shuai, T. Y.; Zheng, L. R.; Tang, H. B.; Zhao, J. W.; Li, G. R. The key role of carboxylate ligands in Ru@Ni-MOFs/NF in promoting water dissociation kinetics for effective hydrogen evolution in alkaline media. *Chem. Eng. J.* **2023**, *451*, 138618.
- [39] Wang, Y.; Wang, C.; Shang, H. Y.; Yuan, M. Y.; Wu, Z. Y.; Li, J.; Du, Y. K. Self-driven Ru-modified NiFe MOF nanosheet as multifunctional electrocatalyst for boosting water and urea electrolysis. *J. Colloid Interface Sci.* **2022**, *605*, 779–789.
- [40] Ding, Z. Q.; Wang, K.; Mai, Z. Q.; He, G. Q.; Liu, Z.; Tang, Z. H. RhRu alloyed nanoparticles confined within metal organic frameworks for electrochemical hydrogen evolution at all pH values. *Int. J. Hydrog. Energy* **2019**, *44*, 24680–24689.
- [41] Sun, Y. M.; Xue, Z. Q.; Liu, Q. L.; Jia, Y. L.; Li, Y. L.; Liu, K.; Lin, Y. Y.; Liu, M.; Li, G. Q.; Su, C. Y. Modulating electronic structure of metal-organic frameworks by introducing atomically dispersed Ru for efficient hydrogen evolution. *Nat. Commun.* **2021**, *12*, 1369.
- [42] Li, Y. W.; Wu, Y. H.; Li, T. T.; Lu, M. T.; Chen, Y.; Cui, Y. J.; Gao, J. K.; Qian, G. D. Tuning the electronic structure of a metal-organic framework for an efficient oxygen evolution reaction by introducing minor atomically dispersed ruthenium. *Carbon Energy* **2023**, *5*, e265.
- [43] Xu, Y.; Yu, S. S.; Ren, T. L.; Liu, S. L.; Wang, Z. Q.; Li, X. N.; Wang, L.; Wang, H. J. Hydrophilic/aerophobic hydrogen-evolving electrode: NiRu-based metal-organic framework nanosheets *in situ* grown on conductive substrates. *ACS Appl. Mater. Interfaces* **2020**, *12*, 34728–34735.
- [44] Zhao, M.; Li, H. L.; Li, W.; Li, J. Y.; Yi, L. Y.; Hu, W. H.; Li, C. M. Ru-doping enhanced electrocatalysis of metal-organic framework nanosheets toward overall water splitting. *Chem.—Eur. J.* **2020**, *26*, 17091–17096.
- [45] Lin, Y.; Zhao, L. X.; Wang, L. M.; Gong, Y. Q. Ruthenium-doped NiFe-based metal-organic framework nanoparticles as highly efficient catalysts for the oxygen evolution reaction. *Dalton Trans.* **2021**, *50*, 4280–4287.
- [46] Liao, P. Q.; Shen, J. Q.; Zhang, J. P. Metal-organic frameworks for electrocatalysis. *Coord. Chem. Rev.* **2018**, *373*, 22–48.
- [47] Xu, Y. X.; Li, Q.; Xue, H. G.; Pang, H. Metal-organic frameworks for direct electrochemical applications. *Coord. Chem. Rev.* **2018**, *376*, 292–318.
- [48] Zhao, S. L.; Tan, C. H.; He, C. T.; An, P. F.; Xie, F.; Jiang, S.; Zhu, Y. F.; Wu, K. H.; Zhang, B. W.; Li, H. J. et al. Structural transformation of highly active metal-organic framework electrocatalysts during the oxygen evolution reaction. *Nat. Energy* **2020**, *5*, 881–890.
- [49] Tian, L.; Li, Z.; Xu, X. N.; Zhang, C. Advances in noble metal (Ru, Rh, and Ir) doping for boosting water splitting electrocatalysis. *J. Mater. Chem. A* **2021**, *9*, 13459–13470.
- [50] Cheng, H. F.; Yang, N. L.; Lu, Q. P.; Zhang, Z. C.; Zhang, H. Syntheses and properties of metal nanomaterials with novel crystal phases. *Adv. Mater.* **2018**, *30*, 1707189.
- [51] Zhao, M.; Chen, Z. T.; Lyu, Z. H.; Hood, Z. D.; Xie, M. H.; Vara, M.; Chi, M. F.; Xia, Y. N. Ru octahedral nanocrystals with a face-centered cubic structure, {111} facets, thermal stability up to 400 °C, and enhanced catalytic activity. *J. Am. Chem. Soc.* **2019**, *141*, 7028–7036.
- [52] Zheng, Y.; Jiao, Y.; Zhu, Y. H.; Li, L. H.; Han, Y.; Chen, Y.; Jaroniec, M.; Qiao, S. Z. High electrocatalytic hydrogen evolution activity of an anomalous ruthenium catalyst. *J. Am. Chem. Soc.* **2016**, *138*, 16174–16181.
- [53] Liu, H. Y.; Chen, L. Y.; Hou, C. C.; Wei, Y. S.; Xu, Q. Soluble porous carbon cage-encapsulated highly active metal nanoparticle catalysts. *J. Mater. Chem. A* **2021**, *9*, 13670–13677.
- [54] Zhao, G. Q.; Rui, K.; Dou, S. X.; Sun, W. P. Heterostructures for electrochemical hydrogen evolution reaction: A review. *Adv. Funct. Mater.* **2018**, *28*, 1803291.
- [55] Zhao, Z. P.; Liu, H. T.; Gao, W. P.; Xue, W.; Liu, Z. Y.; Huang, J.; Pan, X. Q.; Huang, Y. Surface-engineered PtNi-O nanostructure with record-high performance for electrocatalytic hydrogen evolution reaction. *J. Am. Chem. Soc.* **2018**, *140*, 9046–9050.
- [56] Ge, S. M.; Zhang, L. W.; Hou, J. R.; Liu, S.; Qin, Y. J.; Liu, Q.; Cai, X. B.; Sun, Z. Y.; Yang, M. S.; Luo, J. et al. Cu<sub>2</sub>O-derived PtCu nanoalloy toward energy-efficient hydrogen production via hydrazine electrolysis under large current density. *ACS Appl. Energy Mater.* **2022**, *5*, 9487–9494.
- [57] Yang, W. X.; Wang, Z. C.; Zhang, W. Y.; Guo, S. J. Electronic-structure tuning of water-splitting nanocatalysts. *Trends Chem.* **2019**, *1*, 259–271.
- [58] Zhang, Q.; Lian, K.; Liu, Q.; Qi, G. C.; Zhang, S. S.; Luo, J.; Liu, X. J. High entropy alloy nanoparticles as efficient catalysts for alkaline overall seawater splitting and Zn-air batteries. *J. Colloid Interface Sci.* **2023**, *646*, 844–854.
- [59] Zhang, Q.; Lian, K.; Qi, G. C.; Zhang, S. S.; Liu, Q.; Luo, Y.; Luo, J.; Liu, X. J. High-entropy alloys in water electrolysis: Recent advances, fundamentals, and challenges. *Sci. China Mater.* **2023**, *66*, 1681–1701.
- [60] Li, K.; Li, Y.; Wang, Y. M.; Ge, J. J.; Liu, C. P.; Xing, W. Enhanced electrocatalytic performance for the hydrogen evolution reaction through surface enrichment of platinum nanoclusters alloying with ruthenium *in situ* embedded in carbon. *Energy Environ. Sci.* **2018**, *11*, 1232–1239.
- [61] Pedersen, A. F.; Ulrikkeholm, E. T.; Escudero-Escribano, M.; Johansson, T. P.; Malacrida, P.; Pedersen, C. M.; Hansen, M. H.; Jensen, K. D.; Rossmeisl, J.; Friebel, D. et al. Probing the nanoscale structure of the catalytically active overlayer on Pt alloys with rare earths. *Nano Energy* **2016**, *29*, 249–260.

- [62] Cullen, D. A.; More, K. L.; Atanasoska, L. L.; Atanasoski, R. T. Impact of IrRu oxygen evolution reaction catalysts on Pt nanostructured thin films under start-up/shutdown cycling. *J. Power Sources* **2014**, *269*, 671–681.
- [63] Liu, S. L.; Zhang, Q. H.; Bao, J. C.; Li, Y. F.; Dai, Z. H.; Gu, L. Significantly enhanced hydrogen evolution activity of freestanding Pd-Ru distorted icosahedral clusters with less than 600 atoms. *Chem.—Eur. J.* **2017**, *23*, 18203–18207.
- [64] Wang, S.; Li, Z. R.; Shen, T.; Wang, D. L. N-doped carbon shells encapsulated Ru-Ni nanoalloys for efficient hydrogen evolution reaction. *ChemSusChem* **2023**, *16*, e202202128.
- [65] Yu, J.; Dai, Y. W.; Wu, X. H.; Zhang, Z. B.; He, Q. J.; Cheng, C.; Wu, Z.; Shao, Z. P.; Ni, M. Ultrafine ruthenium-iridium alloy nanoparticles well-dispersed on N-rich carbon frameworks as efficient hydrogen-generation electrocatalysts. *Chem. Eng. J.* **2021**, *417*, 128105.
- [66] Zhang, C. H.; Sha, J. W.; Fei, H. L.; Liu, M. J.; Yazdi, S.; Zhang, J. B.; Zhong, Q. F.; Zou, X. L.; Zhao, N. Q.; Yu, H. S. et al. Single-atomic ruthenium catalytic sites on nitrogen-doped graphene for oxygen reduction reaction in acidic medium. *ACS Nano* **2017**, *11*, 6930–6941.
- [67] Zhang, F. F.; Zhu, Y. L.; Lin, Q.; Zhang, L.; Zhang, X. W.; Wang, H. T. Noble-metal single-atoms in thermocatalysis, electrocatalysis, and photocatalysis. *Energy Environ. Sci.* **2021**, *14*, 2954–3009.
- [68] Zhou, L.; Lu, S. Y.; Guo, S. J. Recent progress on precious metal single atom materials for water splitting catalysis. *SusMat* **2021**, *1*, 194–210.
- [69] Zhu, J. T.; Tu, Y. D.; Cai, L. J.; Ma, H. B.; Chai, Y.; Zhang, L. F.; Zhang, W. J. Defect-assisted anchoring of Pt single atoms on MoS<sub>2</sub> nanosheets produces high-performance catalyst for industrial hydrogen evolution reaction. *Small* **2022**, *18*, 2104824.
- [70] Liu, T.; Li, P.; Yao, N.; Cheng, G. Z.; Chen, S. L.; Luo, W.; Yin, Y. D. CoP-doped MOF-based electrocatalyst for pH-universal hydrogen evolution reaction. *Angew. Chem., Int. Ed.* **2019**, *58*, 4679–4684.
- [71] Qiu, T. J.; Liang, Z. B.; Guo, W. H.; Gao, S.; Qu, C.; Tabassum, H.; Zhang, H.; Zhu, B. J.; Zou, R. Q.; Shao-Horn, Y. Highly exposed ruthenium-based electrocatalysts from bimetallic metal-organic frameworks for overall water splitting. *Nano Energy* **2019**, *58*, 1–10.
- [72] Hong, C. B.; Li, X. F.; Wei, W. B.; Wu, X. T.; Zhu, Q. L. Nano-engineering of Ru-based hierarchical porous nanoreactors for highly efficient pH-universal overall water splitting. *Appl. Catal. B: Environ.* **2021**, *294*, 120230.
- [73] Yang, K.; Xu, P. P.; Lin, Z. Y.; Yang, Y.; Jiang, P.; Wang, C. L.; Liu, S.; Gong, S. P.; Hu, L.; Chen, Q. W. Ultrasmall Ru/Cu-doped RuO<sub>2</sub> complex embedded in amorphous carbon skeleton as highly active bifunctional electrocatalysts for overall water splitting. *Small* **2018**, *14*, 1803009.
- [74] Fan, Z. H.; Jiang, J.; Ai, L. H.; Shao, Z. P.; Liu, S. M. Rational design of ruthenium and cobalt-based composites with rich metal-insulator interfaces for efficient and stable overall water splitting in acidic electrolyte. *ACS Appl. Mater. Interfaces* **2019**, *11*, 47894–47903.
- [75] Xu, C.; Yang, X. D.; Wen, X.; Wang, Y. Y.; Sun, Y. Q.; Xu, B.; Li, C. C. Nitrogen-doped carbon encapsulating a RuCo heterostructure for enhanced electrocatalytic overall water splitting. *CrystEngComm* **2022**, *24*, 4208–4214.
- [76] Su, J. W.; Yang, Y.; Xia, G. L.; Chen, J. T.; Jiang, P.; Chen, Q. W. Ruthenium-cobalt nanoalloys encapsulated in nitrogen-doped graphene as active electrocatalysts for producing hydrogen in alkaline media. *Nat. Commun.* **2017**, *8*, 14969.
- [77] Cheng, G. J.; Wu, G. Y.; Li, H.; Liu, S. C.; Liu, Y. Bimetallic oxygen electrocatalyst derived from metallocenes doped MOFs. *Nanotechnology* **2021**, *32*, 225603.
- [78] Sarkar, B.; Das, D.; Nanda, K. K. Construction of noble-metal alloys of cobalt confined N-doped carbon polyhedra toward efficient water splitting. *Green Chem.* **2020**, *22*, 7884–7895.
- [79] Li, G. N.; Zheng, K. T.; Li, W. S.; He, Y. C.; Xu, C. J. Ultralow Ru-induced bimetal electrocatalysts with a Ru-enriched and mixed-valence surface anchored on a hollow carbon matrix for oxygen reduction and water splitting. *ACS Appl. Mater. Interfaces* **2020**, *12*, 51437–51447.
- [80] Xu, Y.; Yin, S. L.; Li, C. J.; Deng, K.; Xue, H. R.; Li, X. N.; Wang, H. J.; Wang, L. Low-ruthenium-content NiRu nanoalloys encapsulated in nitrogen-doped carbon as highly efficient and pH-universal electrocatalysts for the hydrogen evolution reaction. *J. Mater. Chem. A* **2018**, *6*, 1376–1381.
- [81] Wu, W.; Wu, Y.; Zheng, D.; Wang, K.; Tang, Z. H. Ni@Ru core-shell nanoparticles on flower-like carbon nanosheets for hydrogen evolution reaction at all-pH values, oxygen evolution reaction and overall water splitting in alkaline solution. *Electrochim. Acta* **2019**, *320*, 134568.
- [82] Zhang, Z.; Li, P.; Wang, Q.; Feng, Q.; Tao, Y. K.; Xu, J. Y.; Jiang, C.; Lu, X. E.; Fan, J. T.; Gu, M. et al. Mo modulation effect on the hydrogen binding energy of hexagonal-close-packed Ru for hydrogen evolution. *J. Mater. Chem. A* **2019**, *7*, 2780–2786.
- [83] Yang, M. Y.; Jiao, L.; Dong, H. L.; Zhou, L. J.; Teng, C. Q.; Yan, D. M.; Ye, T. N.; Chen, X. X.; Liu, Y.; Jiang, H. L. Conversion of bimetallic MOF to Ru-doped Cu electrocatalysts for efficient hydrogen evolution in alkaline media. *Sci. Bull.* **2021**, *66*, 257–264.
- [84] Chen, J. S.; Huang, J. F.; Wang, R.; Feng, W. H.; Wang, H.; Luo, T. M.; Hu, Y. Z.; Yuan, C. K.; Feng, L. L.; Cao, L. Y. et al. Atomic ruthenium coordinated with chlorine and nitrogen as efficient and multifunctional electrocatalyst for overall water splitting and rechargeable zinc-air battery. *Chem. Eng. J.* **2022**, *441*, 136078.
- [85] Yan, B. L.; Liu, D. P.; Feng, X. L.; Shao, M. Z.; Zhang, Y. Ru species supported on MOF-derived N-doped TiO<sub>2</sub>/C hybrids as efficient electrocatalytic/photocatalytic hydrogen evolution reaction catalysts. *Adv. Funct. Mater.* **2020**, *30*, 2003007.
- [86] Li, D.; Shi, X. L.; Sun, S. C.; Zheng, X. Y.; Tian, D.; Jiang, D. L. Metal-organic framework-derived three-dimensional macropore nitrogen-doped carbon frameworks decorated with ultrafine Ru-based nanoparticles for overall water splitting. *Inorg. Chem.* **2022**, *61*, 9685–9692.
- [87] Qiu, L. S.; Zheng, G. K.; He, Y.; Lei, L. C.; Zhang, X. W. Ultra-small Sn-RuO<sub>2</sub> nanoparticles supported on N-doped carbon polyhedra for highly active and durable oxygen evolution reaction in acidic media. *Chem. Eng. J.* **2021**, *409*, 128155.
- [88] Jiang, P.; Yang, Y.; Shi, R. H.; Xia, G. L.; Chen, J. T.; Su, J. W.; Chen, Q. W. Pt-like electrocatalytic behavior of Ru-MoO<sub>2</sub> nanocomposites for the hydrogen evolution reaction. *J. Mater. Chem. A* **2017**, *5*, 5475–5485.
- [89] Rezaee, S.; Shahrokhian, S. Ruthenium/ruthenium oxide hybrid nanoparticles anchored on hollow spherical copper-cobalt nitride/nitrogen doped carbon nanostructures to promote alkaline water splitting: Boosting catalytic performance via synergy between morphology engineering, electron transfer tuning and electronic behavior modulation. *J. Colloid Interface Sci.* **2022**, *626*, 1070–1084.
- [90] Liu, B.; Shioyama, H.; Akita, T.; Xu, Q. Metal-organic framework as a template for porous carbon synthesis. *J. Am. Chem. Soc.* **2008**, *130*, 5390–5391.
- [91] Bai, X.; Wang, L. M.; Nan, B.; Tang, T. M.; Niu, X. D.; Guan, J. Q. Atomic manganese coordinated to nitrogen and sulfur for oxygen evolution. *Nano Res.* **2022**, *15*, 6019–6025.
- [92] Tang, T. M.; Duan, Z. Y.; Baimanov, D.; Bai, X.; Liu, X. Y.; Wang, L. M.; Wang, Z. L.; Guan, J. Q. Synergy between isolated Fe and Co sites accelerates oxygen evolution. *Nano Res.* **2023**, *16*, 2218–2223.
- [93] Zhu, S. Y.; Ge, J. J.; Liu, C. P.; Xing, W. Atomic-level dispersed catalysts for PEMFCs: Progress and future prospects. *EnergyChem* **2019**, *1*, 100018.
- [94] Liang, Z. B.; Qu, C.; Xia, D. G.; Zou, R. Q.; Xu, Q. Atomically dispersed metal sites in MOF-based materials for electrocatalytic and photocatalytic energy conversion. *Angew. Chem., Int. Ed.* **2018**, *57*, 9604–9633.
- [95] Zhao, C. X.; Li, B. Q.; Liu, J. N.; Zhang, Q. Intrinsic electrocatalytic activity regulation of M-N-C single-atom catalysts for the oxygen reduction reaction. *Angew. Chem., Int. Ed.* **2021**, *60*, 4448–4463.
- [96] Su, J. W.; Ge, R. X.; Jiang, K. M.; Dong, Y.; Hao, F.; Tian, Z. Q.;



- Chen, G. X.; Chen, L. Assembling ultrasmall copper-doped ruthenium oxide nanocrystals into hollow porous polyhedra: Highly robust electrocatalysts for oxygen evolution in acidic media. *Adv. Mater.* **2018**, *30*, 1801351.
- [97] Zhang, H.; Wu, B.; Su, J. W.; Zhao, K. Y.; Chen, L. MOF-derived zinc-doped ruthenium oxide hollow nanorods as highly active and stable electrocatalysts for oxygen evolution in acidic media. *ChemNanoMat* **2021**, *7*, 117–121.
- [98] Lin, Y. C.; Tian, Z. Q.; Zhang, L. J.; Ma, J. Y.; Jiang, Z.; Deibert, B. J.; Ge, R. X.; Chen, L. Chromium-ruthenium oxide solid solution electrocatalyst for highly efficient oxygen evolution reaction in acidic media. *Nat. Commun.* **2019**, *10*, 162.
- [99] Wang, C.; Shang, H. Y.; Li, J.; Wang, Y.; Xu, H.; Wang, C. Y.; Guo, J.; Du, Y. Y. Ultralow Ru doping induced interface engineering in MOF derived ruthenium-cobalt oxide hollow nanobox for efficient water oxidation electrocatalysis. *Chem. Eng. J.* **2021**, *420*, 129805.
- [100] Wang, C.; Qi, L. M. Heterostructured inter-doped ruthenium-cobalt oxide hollow nanosheet arrays for highly efficient overall water splitting. *Angew. Chem., Int. Ed.* **2020**, *59*, 17219–17224.
- [101] Lin, Y.; Zhang, M. L.; Zhao, L. X.; Wang, L. M.; Cao, D. L.; Gong, Y. Q. Ru doped bimetallic phosphide derived from 2D metal organic framework as active and robust electrocatalyst for water splitting. *Appl. Surf. Sci.* **2021**, *536*, 147952.
- [102] Shen, Q. H.; Du, C. C.; Chen, Q. Q.; Tang, J.; Wang, B.; Zhang, X. H.; Chen, J. H. *In-situ* formed Cu-doped RuS<sub>2</sub> hollow polyhedrons integrated with simultaneously heterostructure engineering with metallic Ru for boosting hydrogen evolution in alkaline media. *Mater. Today Phys.* **2022**, *23*, 100625.
- [103] Liu, Y.; Xu, S. J.; Zheng, X. Y.; Lu, Y. K.; Li, D.; Jiang, D. L. Ru-doping modulated cobalt phosphide nanoarrays as efficient electrocatalyst for hydrogen evolution reaction. *J. Colloid Interface Sci.* **2022**, *625*, 457–465.
- [104] Chen, H. H.; Zhang, S. S.; Liu, Q.; Yu, P.; Luo, J.; Hu, G. Z.; Liu, X. J. CoSe<sub>2</sub> nanocrystals embedded into carbon framework as efficient bifunctional catalyst for alkaline seawater splitting. *Inorg. Chem. Commun.* **2022**, *146*, 110170.
- [105] Qiu, B. C.; Zhang, Y. F.; Guo, X. Y.; Ma, Y. X.; Du, M. M.; Fan, J.; Zhu, Y.; Zeng, Z. Y.; Chai, Y. Nitrogen-induced interfacial electronic structure of NiS<sub>2</sub>/CoS<sub>2</sub> with optimized water and hydrogen binding abilities for efficient alkaline hydrogen evolution electrocatalysis. *J. Mater. Chem. A* **2022**, *10*, 719–725.
- [106] Wang, P.; Luo, Y. Z.; Zhang, G. X.; Chen, Z. S.; Ranganathan, H.; Sun, S. H.; Shi, Z. C. Interface engineering of Ni<sub>x</sub>S<sub>y</sub>@MnO<sub>x</sub>H<sub>y</sub> nanorods to efficiently enhance overall-water-splitting activity and stability. *Nano-Micro Lett.* **2022**, *14*, 120.
- [107] Zhou, J.; Dou, Y. B.; Wu, X. Q.; Zhou, A.; Shu, L.; Li, J. R. Alkali-etched Ni(II)-based metal-organic framework nanosheet arrays for electrocatalytic overall water splitting. *Small* **2020**, *16*, 1906564.
- [108] Liu, D. M.; Wang, C.; Zhou, Z. M.; Ye, C. Q.; Yu, R.; Wang, C. Q.; Du, Y. K. Ultra-low Ru doped MOF-derived hollow nanorods for efficient oxygen evolution reaction. *Inorg. Chem. Front.* **2022**, *9*, 6158–6166.
- [109] Liu, D. M.; Xu, H.; Wang, C.; Ye, C. Q.; Yu, R.; Du, Y. K. *In situ* etch engineering of Ru doped NiFe(OH)<sub>x</sub>/NiFe-MOF nanocomposites for boosting the oxygen evolution reaction. *J. Mater. Chem. A* **2021**, *9*, 24670–24676.
- [110] Hu, Y. D.; Luo, G.; Wang, L. G.; Liu, X. K.; Qu, Y. T.; Zhou, Y. S.; Zhou, F. Y.; Li, Z. J.; Li, Y. F.; Yao, T. et al. Single Ru atoms stabilized by hybrid amorphous/crystalline FeCoNi layered double hydroxide for ultraefficient oxygen evolution. *Adv. Energy Mater.* **2021**, *11*, 2002816.
- [111] Luo, R.; Li, Z. Y.; Li, R. X.; Jiang, C. L.; Qi, R. J.; Liu, M. Q.; Lin, H. C.; Huang, R.; Luo, C. H.; Peng, H. Ultrafine Ru nanoparticles derived from few-layered Ti<sub>3</sub>C<sub>2</sub>T<sub>x</sub> MXene templated MOF for highly efficient alkaline hydrogen evolution. *Int. J. Hydron. Energy* **2022**, *47*, 32787–32795.
- [112] Li, J. Z.; Hou, C. Z.; Chen, C.; Ma, W. S.; Li, Q.; Hu, L. W.; Lv, X. W.; Dang, J. Collaborative interface optimization strategy guided ultrafine RuCo and MXene heterostructure electrocatalysts for efficient overall water splitting. *ACS Nano* **2023**, *17*, 10947–10957.
- [113] Deeloed, W.; Priamushko, T.; Čížek, J.; Suramitr, S.; Kleitz, F. Defect-engineered hydroxylated mesoporous spinel oxides as bifunctional electrocatalysts for oxygen reduction and evolution reactions. *ACS Appl. Mater. Interfaces* **2022**, *14*, 23307–23321.
- [114] Zou, Z. H.; Cai, M. M.; Zhao, X. H.; Huang, J. F.; Du, J.; Xu, C. L. Defective metal-organic framework derivative by room-temperature exfoliation and reduction for highly efficient oxygen evolution reaction. *J. Mater. Chem. A* **2019**, *7*, 14011–14018.
- [115] Wu, X. K.; Xu, W. X.; Wang, Z. C.; Li, H. D.; Wang, M. H.; Zhang, D.; Lai, J. P.; Wang, L. Rapid microwave synthesis of Ru-supported partially carbonized conductive metal-organic framework for efficient hydrogen evolution. *Chem. Eng. J.* **2022**, *431*, 133247.
- [116] Bai, X.; Duan, Z. Y.; Nan, B.; Wang, L. M.; Tang, T. M.; Guan, J. Q. Unveiling the active sites of ultrathin Co-Fe layered double hydroxides for the oxygen evolution reaction. *Chin. J. Catal.* **2022**, *43*, 2240–2248.
- [117] Kong, X.; Gao, Q. L.; Bu, S. Y.; Xu, Z. A.; Shen, D.; Liu, B.; Lee, C. S.; Zhang, W. J. Plasma-assisted synthesis of nickel-cobalt nitride-oxide hybrids for high-efficiency electrochemical hydrogen evolution. *Mater. Today Energy* **2021**, *21*, 100784.
- [118] Bai, X.; Guan, J. Q. MXenes for electrocatalysis applications: Modification and hybridization. *Chin. J. Catal.* **2022**, *43*, 2057–2090.
- [119] Das, S.; Heasman, P.; Ben, T.; Qiu, S. L. Porous organic materials: Strategic design and structure-function correlation. *Chem. Rev.* **2017**, *117*, 1515–1563.
- [120] Ding, S. Y.; Wang, W. Covalent organic frameworks (COFs): From design to applications. *Chem. Soc. Rev.* **2013**, *42*, 548–568.
- [121] Liu, M. Y.; Guo, L. P.; Jin, S. B.; Tan, B. E. Covalent triazine frameworks: Synthesis and applications. *J. Mater. Chem. A* **2019**, *7*, 5153–5172.
- [122] Tan, L. X.; Tan, B. E. Hypercrosslinked porous polymer materials: Design, synthesis, and applications. *Chem. Soc. Rev.* **2017**, *46*, 3322–3356.
- [123] Cooper, A. I. Conjugated microporous polymers. *Adv. Mater.* **2009**, *21*, 1291–1295.
- [124] Budd, P. M.; Ghanem, B. S.; Makhseed, S.; McKeown, N. B.; Msayib, K. J.; Tattershall, C. E. Polymers of intrinsic microporosity (PIMs): Robust, solution-processable, organic nanoporous materials. *Chem. Commun.* **2004**, 230–231.
- [125] Yang, C. H.; Yang, Z. D.; Dong, H.; Sun, N.; Lu, Y.; Zhang, F. M.; Zhang, G. L. Theory-driven design and targeting synthesis of a highly-conjugated basal-plane 2D covalent organic framework for metal-free electrocatalytic OER. *ACS Energy Lett.* **2019**, *4*, 2251–2258.
- [126] Aiyappa, H. B.; Thote, J.; Shinde, D. B.; Banerjee, R.; Kurungot, S. Cobalt-modified covalent organic framework as a robust water oxidation electrocatalyst. *Chem. Mater.* **2016**, *28*, 4375–4379.
- [127] Chandran, R. K.; Illathvalappil, R. R.; Wakchaure, V. C.; Goudappagouda; Kurungot, S.; Babu, S. S. Metalloporphyrin two-dimensional polymers via metal-catalyst-free C–C bond formation for efficient catalytic hydrogen evolution. *ACS Appl. Energy Mater.* **2018**, *1*, 6442–6450.
- [128] Fang, H. B.; Chen, J. X.; Balogun, M. S.; Tong, Y. X.; Zhang, J. Y. Covalently modified electrode with Pt nanoparticles encapsulated in porous organic polymer for efficient electrocatalysis. *ACS Appl. Nano Mater.* **2018**, *1*, 6477–6482.
- [129] Jia, H. X.; Sun, Z. J.; Jiang, D. C.; Du, P. W. Covalent cobalt porphyrin framework on multiwalled carbon nanotubes for efficient water oxidation at low overpotential. *Chem. Mater.* **2015**, *27*, 4586–4593.
- [130] Boro, B.; Adak, M. K.; Biswas, S.; Sarkar, C.; Nailwal, Y.; Shrotri, A.; Chakraborty, B.; Wong, B. M.; Mondal, J. Electrocatalytic water oxidation performance in an extended porous organic framework with a covalent alliance of distinct Ru sites. *Nanoscale* **2022**, *14*, 7621–7633.
- [131] Pan, R. P.; Wu, J. L.; Wang, W. W.; Cheng, C.; Liu, X. K. Robust crystalline aromatic imide-linked two-dimensional covalent organic frameworks confining ruthenium nanoparticles as efficient hydrogen evolution electrocatalyst. *Colloids Surf. A: Physicochem. Eng. Asp.* **2021**, *621*, 126511.

- [132] Maiti, S.; Chowdhury, A. R.; Das, A. K. Electrochemically facile hydrogen evolution using ruthenium encapsulated two dimensional covalent organic framework (2D COF). *ChemNanoMat* **2019**, *6*, 99–106.
- [133] Zhao, Q.; Chen, S. H.; Ren, H. W.; Chen, C.; Yang, W. Ruthenium nanoparticles confined in covalent organic framework/reduced graphene oxide as electrocatalyst toward hydrogen evolution reaction in alkaline media. *Ind. Eng. Chem. Res.* **2021**, *60*, 11070–11078.
- [134] Zhao, Y. X.; Liang, Y.; Wu, D. X.; Tian, H.; Xia, T.; Wang, W. X.; Xie, W. Y.; Hu, X. M.; Tian, X. L.; Chen, Q. Ruthenium complex of  $sp^2$  carbon-conjugated covalent organic frameworks as an efficient electrocatalyst for hydrogen evolution. *Small* **2022**, *18*, 2107750.
- [135] Gao, X.; Gao, Y. J.; Li, S. Q.; Yang, J.; Zhuang, G. L.; Deng, S. W.; Yao, Z. H.; Zhong, X.; Wei, Z. Z.; Wang, J. G. Defect CTF derived Ru-based catalysts for high performance overall water splitting reaction. *J. Energy Chem.* **2020**, *50*, 135–142.
- [136] Xu, C. L.; Wang, H.; Wang, Q.; Wang, Y.; Zhang, Y.; Fan, G. Y. Ruthenium coordinated with triphenylphosphine-hyper-crosslinked polymer: An efficient catalyst for hydrogen evolution reaction and hydrolysis of ammonia borane. *Appl. Surf. Sci.* **2019**, *466*, 193–201.
- [137] Ma, R. P.; Wang, X.; Yang, X. L.; Li, Y.; Liu, C. P.; Ge, J. J.; Xing, W. Identification of active sites and synergistic effect in multicomponent carbon-based Ru catalysts during electrocatalytic hydrogen evolution. *Nano Res.* **2023**, *16*, 166–173.
- [138] Stegbauer, L.; Schwinghammer, K.; Lotsch, B. V. A hydrazone-based covalent organic framework for photocatalytic hydrogen production. *Chem. Sci.* **2014**, *5*, 2789–2793.
- [139] Zhang, J.; Wang, L. B.; Li, N.; Liu, J. F.; Zhang, W.; Zhang, Z. B.; Zhou, N. C.; Zhu, X. L. A novel azobenzene covalent organic framework. *CrystEngComm* **2014**, *16*, 6547–6551.
- [140] Zhao, X. J.; Pachfule, P.; Li, S.; Langenhahn, T.; Ye, M. Y.; Schlesiger, C.; Praetz, S.; Schmidt, J.; Thomas, A. Macro/microporous covalent organic frameworks for efficient electrocatalysis. *J. Am. Chem. Soc.* **2019**, *141*, 6623–6630.
- [141] Bhunia, S.; Das, S. K.; Jana, R.; Peter, S. C.; Bhattacharya, S.; Addicoat, M.; Bhaumik, A.; Pradhan, A. Electrochemical stimuli-driven facile metal-free hydrogen evolution from pyrene-porphyrin-based crystalline covalent organic framework. *ACS Appl. Mater. Interfaces* **2017**, *9*, 23843–23851.
- [142] Tang, T. M.; Li, S. S.; Sun, J. R.; Wang, Z. L.; Guan, J. Q. Advances and challenges in two-dimensional materials for oxygen evolution. *Nano Res.* **2022**, *15*, 8714–8750.
- [143] Ji, J.; Zhang, C. J.; Qin, S. B.; Jin, P. First-principles investigation of two-dimensional covalent-organic framework electrocatalysts for oxygen evolution/reduction and hydrogen evolution reactions. *Sustainable Energy Fuels* **2021**, *5*, 5615–5626.
- [144] Zhou, Y. N.; Chen, L. L.; Sheng, L.; Luo, Q. Q.; Zhang, W. H.; Yang, J. L. Dual-metal atoms embedded into two-dimensional covalent organic framework as efficient electrocatalysts for oxygen evolution reaction: A DFT study. *Nano Res.* **2022**, *15*, 7994–8000.
- [145] Zhuang, X. D.; Zhao, W. X.; Zhang, F.; Cao, Y.; Liu, F.; Bi, S.; Feng, X. L. A two-dimensional conjugated polymer framework with fully  $sp^2$ -bonded carbon skeleton. *Polym. Chem.* **2016**, *7*, 4176–4181.
- [146] Kuhn, P.; Antonietti, M.; Thomas, A. Porous, covalent triazine-based frameworks prepared by ionothermal synthesis. *Angew. Chem., Int. Ed.* **2008**, *47*, 3450–3453.
- [147] Jiao, L.; Hu, Y. L.; Ju, H. X.; Wang, C. D.; Gao, M. R.; Yang, Q.; Zhu, J. F.; Yu, S. H.; Jiang, H. L. From covalent triazine-based frameworks to N-doped porous carbon/reduced graphene oxide nanosheets: Efficient electrocatalysts for oxygen reduction. *J. Mater. Chem. A* **2017**, *5*, 23170–23178.
- [148] Davankov, V. A.; Rogoshin, S. V.; Tsyrupa, M. P. Macromet isoporous gels through crosslinking of dissolved polystyrene. *J. Polym. Sci., Polym. Symp.* **1974**, *47*, 95–101.
- [149] Tsyrupa, M. P.; Davankov, V. A. Porous structure of hypercrosslinked polystyrene: State-of-the-art mini-review. *React. Funct. Polym.* **2006**, *66*, 768–779.